Inflammasomes within Hyperactive Murine Dendritic Cells Stimulate Long-Lived T Cell-Mediated Anti-tumor Immunity

Cell Reports

Article

Inflammasomes within Hyperactive Murine Dendritic Cells Stimulate Long-Lived T Cell-Mediated Anti-tumor Immunity

Graphical Abstract

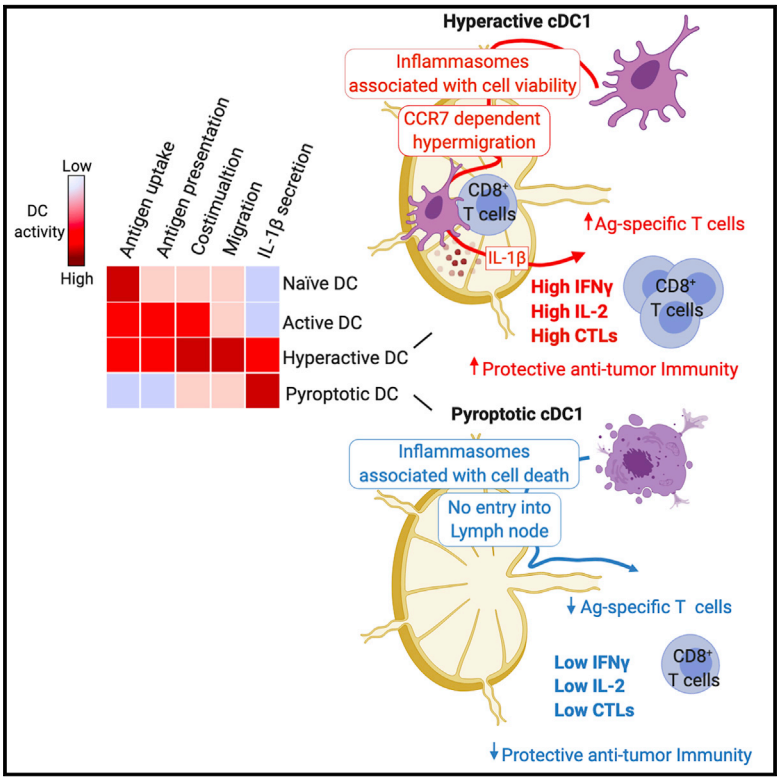

Highlights

- Hyperactive dendritic cells display enhanced ability to migrate to lymph nodes
- Hyperactive dendritic cells retain inflammasome activity in the dLN
- Hyperactive cDC1s induce long-lived $CD8^+$ T-cell-mediated anti-tumor immunity
- Hyperactivating stimuli eradicate tumors that are resistant to anti-PD1 therapy

Authors

Dania Zhivaki, Francesco Borriello, Ohn A. Chow, ..., Caroline L. Sokol, Ivan Zanoni, Jonathan C. Kagan

Correspondence

jonathan.kagan@childrens.harvard.edu

In Brief

Inflammasome activation in dendritic cells (DCs) leads to pyroptosis or hyperactivation. Zhivaki et al. show that in contrast to pyroptotic DCs, hyperactive DCs stimulate durable anti-tumor immunity that eradicates established tumors. These protective responses are intrinsic to cDC1 cells and depend on DC hypermigration and on the inflammasome-dependent cytokine IL-1β.

Zhivaki et al., 2020, Cell Reports *33*, 108381
November 17, 2020
https://doi.org/10.1016/j.celrep.2020.108381

Cell Reports

CellPress
OPEN ACCESS

Article

Inflammasomes within Hyperactive Murine Dendritic Cells Stimulate Long-Lived T Cell-Mediated Anti-tumor Immunity

Dania Zhivaki,[1] Francesco Borriello,[2,9] Ohn A. Chow,[3] Benjamin Doran,[6,7,8] Ira Fleming,[6,7,8] Derek J. Theisen,[4] Paris Pallis,[5] Alex K. Shalek,[6,7,8] Caroline L. Sokol,[3] Ivan Zanoni,[1,2] and Jonathan C. Kagan[1,10,*]

[1]Harvard Medical School and Division of Gastroenterology, Boston Children's Hospital, Boston, MA, USA
[2]Harvard Medical School and Division of Immunology, Boston Children's Hospital, Boston, MA, USA
[3]Center for Immunology & Inflammatory Diseases, Division of Rheumatology, Allergy & Immunology, Massachusetts General Hospital, Harvard Medical School, Boston, MA 02114, USA
[4]Department of Pathology and Immunology, Washington University School of Medicine, St. Louis, MO, USA
[5]Department of Immunology, Harvard Medical School, Boston, MA 02115, USA
[6]Department of Chemistry, Institute for Medical Engineering and Sciences (IMES), Koch Institute for Integrative Cancer Research, MIT, Cambridge, MA 02142, USA
[7]Ragon Institute of MGH, Harvard, and MIT, Cambridge, MA 02139, USA
[8]Broad Institute of MIT and Harvard, Cambridge, MA 02142, USA
[9]Department of Translational Medical Sciences and Center for Basic and Clinical Immunology Research (CISI), University of Naples Federico II, Naples, Italy
[10]Lead Contact
*Correspondence: jonathan.kagan@childrens.harvard.edu
https://doi.org/10.1016/j.celrep.2020.108381

SUMMARY

Central to anti-tumor immunity are dendritic cells (DCs), which stimulate long-lived protective T cell responses. Recent studies have demonstrated that DCs can achieve a state of hyperactivation, which is associated with inflammasome activities within living cells. Herein, we report that hyperactive DCs have an enhanced ability to migrate to draining lymph nodes and stimulate potent cytotoxic T lymphocyte (CTL) responses. This enhanced migratory activity is dependent on the chemokine receptor CCR7 and is associated with a unique transcriptional program that is not observed in conventionally activated or pyroptotic DCs. We show that hyperactivating stimuli are uniquely capable of inducing durable CTL-mediated anti-tumor immunity against tumors that are sensitive or resistant to PD-1 inhibition. These protective responses are intrinsic to the cDC1 subset of DCs, depend on the inflammasome-dependent cytokine IL-1β, and enable tumor lysates to serve as immunogens. If these activities are verified in humans, hyperactive DCs may impact immunotherapy.

INTRODUCTION

Central to our understanding of protective immunity to infection and cancer are dendritic cells (DCs), which patrol the tissues of the body (Alvarez et al., 2008). DCs survey the environment for threats to the host through the actions of pattern recognition receptors (PRRs), which recognize microbial products or host-encoded molecules indicative of tissue injury (Janeway and Medzhitov, 2002; Brubaker et al., 2015). Microbial ligands for PRRs are classified as pathogen-associated molecular patterns (PAMPs), whereas host-derived PRR ligands are damage-associated molecular patterns (DAMPs) (Matzinger, 2002).

Upon detection of PAMPs, PRRs unleash signaling pathways that shift DC activities from a non-stimulatory (naive) state to an "activated" state (Inaba et al., 2000; Mellman and Steinman, 2001). Active DCs have a life expectancy of a few days and are equipped to prime T cells and boost antigen-specific T cell responses. As such, numerous strategies have been undertaken to promote DC activation via Toll-like receptor (TLR) agonists to drive protective anti-tumor immunity (Sabado et al., 2017). Notably, TLRs alone do not upregulate all the signals needed by DCs to promote T cell-mediated immunity. Members of the interleukin-1 (IL-1) family of cytokines are regulators of T cell differentiation, long-lived memory T cell generation, and effector function (Ben-Sasson et al., 2009, 2013; Garlanda et al., 2013; Jain et al., 2018; Lee et al., 2019). The expression of IL-1β is induced by TLRs, but this cytokine lacks an N-terminal secretion signal and is therefore not released from cells via the conventional biosynthetic pathway (Garlanda et al., 2013). Rather, IL-1β accumulates in an inactive state in the cytosol.

To induce IL-1β release, most cells require a second signal that stimulates pyroptosis. Pyroptosis is a regulated process that results from the actions of inflammasomes, which are supramolecular organizing centers (SMOCs) that assemble in the

cytosol (Kagan et al., 2014; Lu et al., 2014). Inflammasome assembly is commonly stimulated upon detection of PAMPs or DAMPs by cytosolic PRRs (Lamkanfi and Dixit, 2014; Kieser and Kagan, 2017). Pyroptosis leads to the release of IL-1 family members, thereby providing signals to T cells that TLRs cannot offer. Despite this gain in activity, in terms of promoting IL-1β release, pyroptotic cells are dead and lose the ability to participate in the days-long process needed to stimulate and differentiate naive T cells in the draining lymph node (dLN) (Mempel et al., 2004). Indeed, stimuli that promote pyroptosis, such as the vaccine adjuvant alum (Eisenbarth et al., 2008; Kool et al., 2008a), are weak inducers of T cell-mediated protective immunity (Marrack et al., 2009).

We reasoned that the ideal strategy to stimulate robust T cell immunity would be to combine the benefits of activated and pyroptotic DCs, whereby DCs would have the ability to release IL-1β while maintaining viability. We recently identified a new activation state of DCs that displays these attributes. When DCs are exposed to PAMPs (e.g., TLR ligands) and a collection of oxidized phospholipids released from dying cells (DAMPs), the cells achieve a long-lived state of "hyperactivation" (Zanoni et al., 2016, 2017). The collection of oxidized lipids is known as oxPAPC (oxidized 1-palmitoyl-2-arachidonyl-sn-glycero-3-phosphorylcholine), and individual components such as PGPC (1-palmitoyl-2-glutaryl-sn-glycero-3-phosphocholine) can induce a hyperactive state in bone-marrow-derived DCs (BMDCs) (Zanoni et al., 2016). Hyperactive cells display the activities of activated DCs, in terms of cytokine release (e.g., tumor necrosis factor alpha [TNF-α]), but they have also gained the ability to release IL-1β over the course of several days (Zanoni et al., 2017).

Mechanisms underlying the hyperactive state of DCs have been defined, as oxPAPC binds and stimulates the cytosolic PRR caspase-11 (Zanoni et al., 2016). Caspase-11 binding results in the activation of NLRP3 (NLR family pyrin domain containing 3) and the assembly of an inflammasome that does not lead to pyroptosis, but rather leads to the release of IL-1β from living cells. IL-1β release from hyperactive cells is mediated by the pore-forming protein gasdermin D (Kayagaki et al., 2015; Aglietti et al., 2016; Liu et al., 2016; Evavold et al., 2017). The impact of hyperactive cells on adaptive immunity is poorly defined.

Herein, we report that oxidized phospholipids that hyperactivate DCs induce strong cytotoxic T lymphocyte (CTL) responses, which endow hyperactive DCs with the ability to mediate long-term protective anti-tumor immunity, even when a complex antigen source is used (e.g., tumor cell lysates). Hyperactivation-mediated protection is mediated by the cDC1 subset of DCs, which depend on inflammasome-dependent IL-1β release and on an enhanced ability to migrate to the dLN. These findings establish the physiological importance of the hyperactive state of DC1s in protective immunity to cancer.

RESULTS

Oxidized Phospholipids Induce a State of Hyperactivation in cDC1s and cDC2s

Several studies have assessed phagocyte hyperactivation, but those focused on DCs have used monocyte-like BMDCs that were generated with granulocyte-macrophage colony-stimulating factor (GM-CSF) (Chen et al., 2014; Gaidt et al., 2016; Wolf et al., 2016; Zanoni et al., 2016; Monteleone et al., 2018). To determine if conventional DCs (cDCs) can achieve a hyperactive state, we used DCs that were differentiated from BM using Fms-like tyrosine kinase 3 ligand (FLT3L). FLT3L-DCs were primed with LPS (lipopolysaccharide) and then treated with the oxidized phospholipids oxPAPC or PGPC. Alternatively, FLT3L-DCs were stimulated with the traditional activation stimulus LPS or were primed with LPS and treated with the pyroptotic stimulus alum. LPS treatment did not induce IL-1β release from DCs, whereas pyroptotic DCs released IL-1β into the extracellular space (Figure 1A, left panel). As expected, IL-1β secretion was co-incident with cell death in pyroptotic DCs, as assessed by the release of the cytosolic enzyme lactate dehydrogenase (LDH) (Figure 1A, middle panel). Stimulation with the hyperactivating stimuli LPS plus PGPC induced dose-dependent IL-1β secretion from DCs in the absence of LDH release (Figures 1A and S1A). Dose responses of DCs treated with various concentrations of LPS and PGPC identified conditions that were used in this study, where maximal levels of IL-1β release correlated with inflammatory markers in DCs (e.g., TNF-α secretion) (Figure S1A). We noted a cell-type-specific behavior of the oxPAPC mixture, as compared to the pure component PGPC. In contrast to PGPC, which induced robust IL-1β release from all DCs, oxPAPC was a strong inducer of IL-1β release from GMCSF-DCs but a weak inducer of IL-1β release from FL3TL-DCs (Figures 1A, S1A, and S1B). IL-1β release from pyroptotic or hyperactive DCs was in both cases dependent on the inflammasome components NLRP3 and caspases 1 and 11 (Figure 1A). Similar behaviors of DCs were observed when DCs were primed with the unmethylated cytosine-phosphate-guanine (CpG) DNA (Figure S1C).

cDCs are divided into two major subsets: cDC1s and cDC2s. Of these subsets, cDC1s are uniquely capable of antigen cross-presentation and can prime naive $CD8^+$ T cells, but also $CD4^+$ T cells (Cancel et al., 2019; Theisen et al., 2019; Ferris et al., 2020). In contrast, cDC2s activate Th2 and Th17 immunity. To determine if the behavior of hyperactive DCs extends to cDC1 or cDC2 subsets, we isolated cDC1s or cDC2s from FLT3L-differentiated DCs (Figure S1D). Similar to the behavior of bulk FLT3L-derived DCs, treatment with LPS plus PGPC led to TNF-α and IL-1β release from FLT3L-cDC1s and cDC2s in the absence of cell death (Figure 1B). oxPAPC exhibited toxic effects on cDC1s, but not cDC2s (Figure 1B). Based on the uniformity of DC responses to PGPC, we focused much of our subsequent work on the activities of PGPC as an inducer of cDC1 and cDC2 hyperactivation.

Hyperactive cDCs Display a Hypermigratory Phenotype

We observed that hyperactive cDC1s stimulated with LPS plus PGPC displayed highly extended membrane protrusions, as compared to naive or active DCs, which suggested potential changes in migratory activity (Figure 1C). RNA sequencing of cDC1s and cDC2s, stimulated with LPS alone or with LPS plus PGPC, revealed upregulated gene signatures that include migration-related clusters involved in DC chemotaxis, actin polymerization, and DC migration (GEO: GSE156159) (Figure 1D; Table S1). Interestingly, in addition to the common signatures shared

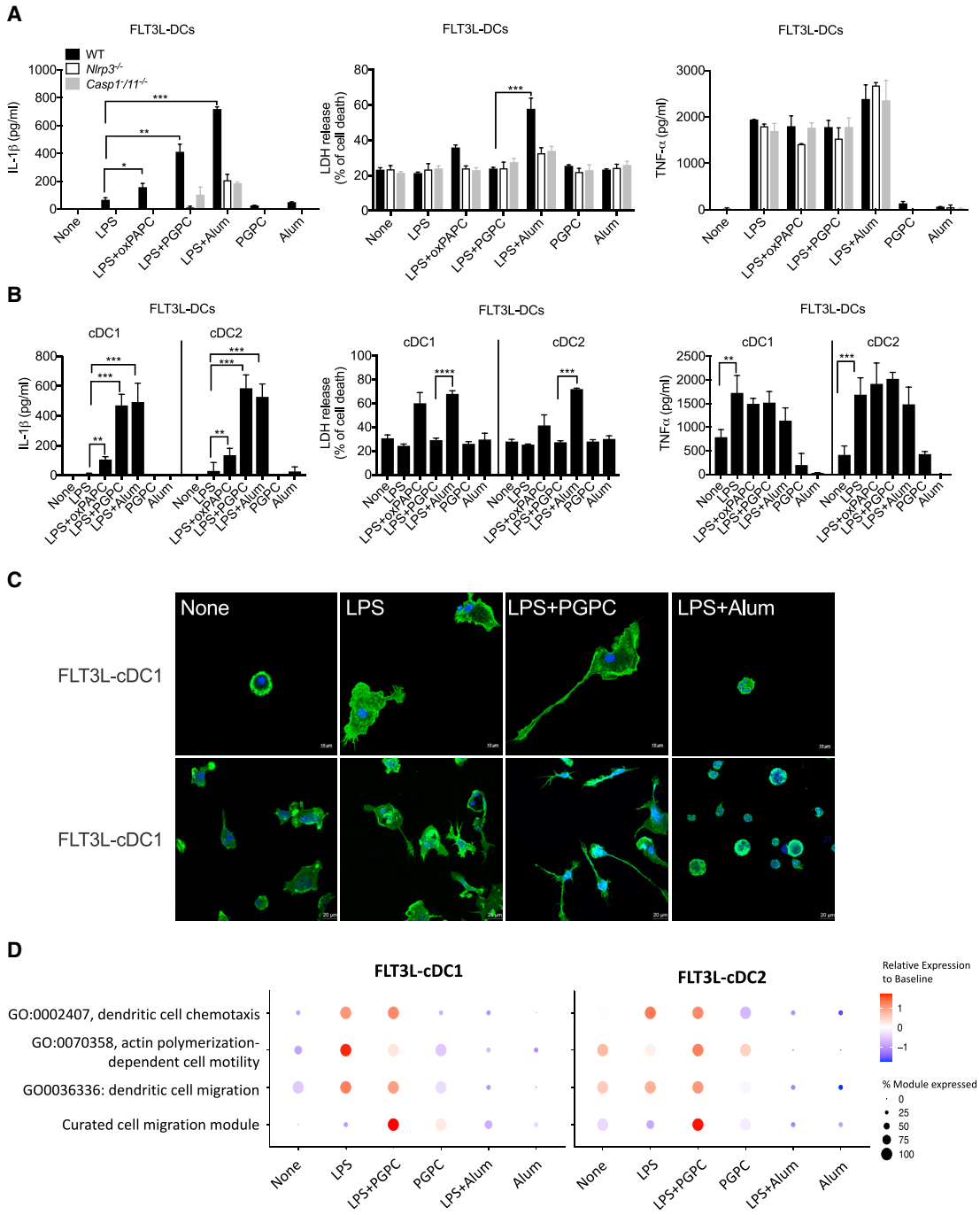

Figure 1. Oxidized Phospholipids Induce a State of Hyperactivation in cDC1s and cDC2s

(A and B) BMDCs, cDC1s, or cDC2s (as indicated) were either left untreated ("None") or treated with indicated stimuli. IL-1β and TNF-α release was monitored by ELISA. Cell death was measured by LDH release. Means and SDs from three replicates are shown, and data are representative of at least three independent experiments.

(C) Immunofluorescence staining of phalloidin (green) and DAPI (blue) for cDC1s. Scale bars: 10 μm (upper panel) and 20 μm (lower panel).

(D) cDC1s and cDC2s were either left untreated ("None") or treated as indicated prior to RNA sequencing (n = 3 mice). Shown is the expression of mouse Gene Ontology modules. Color of dot represents the average relative increase or decrease of log-normalized expression from randomized modules of same number genes. Size of dot shows percent of module expressed by samples. p values of < 0.05 (*), < 0.01 (**), < 0.001 (***), or, ≤ 0.0001 (****) are indicated.

by active and hyperactive DCs, hyperactive cDC1s and cDC2s upregulated an exclusive gene signature that we named "curated cell migration module," since this gene set mainly encompasses genes whose products control cell migration (e.g., *Rhob*, *Rhoc*, *Rac1*, *Arpin*, *L1cam*) (Figures 1D and S2A; Table S1). These data prompted an exploration of DC motility. We tracked the motility of single cells and the collective motion of naive, active, or hyperactive DCs stimulated with LPS plus PGPC on a glass surface. A measurement of straightness index, the total cell displacement from its starting point compared to the distance traveled by the cell, revealed that hyperactive DCs exhibited the highest movement and directionality, as compared to their naive or active counterparts (Figure 2A; Videos S1, S2, and S3). Furthermore, we noted that LPS plus PGPC—and to a lesser extent, LPS plus oxPAPC—strongly induced the upregulation of the chemokine receptor CCR7 in living cDC1 and cDC2 subsets as compared to their naive, active, and pyroptotic counterparts (Figures 2B and S2B). CCR7 upregulation coincides with migratory capacity of DCs from the skin to the dLN (Martín-Fontecha et al., 2003; Ohl et al., 2004; Alvarez et al., 2008). To determine if hyperactive DCs displayed an enhanced ability to migrate to the dLN, we performed an adoptive cell transfer of carboxyfluorescein succinimidyl ester (CFSE)-labeled CD45.2$^+$ FLT3L-DCs that were previously untreated, pre-treated with LPS for 15 h, or primed with LPS for 3 h then treated with PGPC or oxPAPC or alum for 12 h. Live DCs were injected subcutaneously (s.c.) into wild-type (WT) CD45.1 mice. Fifteen hours post-DC injection, we measured the absolute number of fluorescent DCs recovered from the adjacent skin dLN as CD45.2$^+$ CFSE$^+$ among CD11c$^+$ live cells. Notably, DCs that were stimulated with LPS plus PGPC exhibited the strongest ability to emigrate to the dLN (Figure 2C). Hyperactive DCs that lack CCR7 demonstrated a reduced migratory capacity to the skin dLN (Figure 2C). *Nlrp3*$^{-/-}$ DCs maintained a strong emigration capacity from the skin to the skin dLN, indicating that hyperactivation-mediated hypermigratory capacity is independent of inflammasome activity (Figure 2C). In summary, these data demonstrate that in addition to releasing IL-1β while maintaining viability, hyperactive DCs display a hypermigratory phenotype that enables their enhanced accumulation in adjacent dLN.

To assess whether hyperactive DCs retained the ability to produce IL-1β after migration to the dLN, we sorted from the skin dLN WT or *Nlrp3*$^{-/-}$ hyperactive DCs as CD11c$^+$ CD45.2$^+$ CFSE$^+$ live cells (Figures S2C and S2D) and resident DCs as CD11c$^+$ CFSE^{neg} DCs. We then measured IL-1β in the extracellular media 24 h post-sorting without any further stimulation. Resident DCs or *Nlrp3*$^{-/-}$ DCs stimulated with LPS plus PGPC that migrated to the dLN were unable to secrete IL-1β (Figure 2D). Conversely, WT hyperactive DCs that migrated to the dLN secreted IL-1β in the absence of LDH release (Figure 2D). To further assess their inflammasome activity, we determined the percentage of hyperactive DCs in the dLN that harbor ASC (Apoptosis-associated speck-like protein containing a CARD) specks, a hallmark of inflammasome activation. We sorted hyperactive DCs or resident DCs based on differential staining of CD45.1 and CD45.2. We used two strategies to detect ASC specks in DCs: we stained endogenous ASC in hyperactive WT or *Nlrp3*$^{-/-}$ DCs that migrated to the dLN and in resident DCs immediately post-sorting (Figure 2E), or we used FLT3L-DCs from mice that constitutively express ASC-citrine transgene (Tzeng et al., 2016) (Figure S2E). We found that 40% of WT hyperactive DCs sorted from the dLN harbored ASC specks, as detected by confocal microscopy, while 1% of *Nlrp3*$^{-/-}$ or resident DCs harbored ASC specks in the dLN (Figure 2E). Furthermore, 20% of ASC-citrine DCs stimulated with LPS plus PGPC that have migrated to the dLN harbored perinuclear ASC specks, as well as ASC specks located in the long DC protrusions (Figure S2E). Overall, these results establish that hyperactivating stimuli induce inflammasome-dependent IL-1β release from hyperactive DCs that display an enhanced ability to migrate to dLN.

Hyperactive DCs Potentiate CTL Responses in an Inflammasome-Dependent Manner

RNA sequencing indicated that FLT3L-cDC1s and cDC2s upregulated many genes involved in positively regulating CD8$^+$ T cell responses (Figure S3A; Table S1). To address whether hyperactive DCs can enhance antigen-specific CD8$^+$ T cell responses, we s.c. transferred DCs that were treated as described above and loaded with ovalbumin (OVA), then measured endogenous OVA-specific CD8$^+$ T cells in the dLN 7 days post-DC injection. Active and hyperactive DCs were able to uptake fluorescent OVA (OVA-FITC) to a similar extent, whereas pyroptotic DCs exhibited reduced OVA internalization capacity (Figure S3B). In addition, we found that active and hyperactive DCs exhibited enhanced cross-presentation of the OVA-derived peptide SIINFEKL on H2^{kb} molecules following OVA protein internalization, as compared to their naive or pyroptotic counterparts (Figure S3C). Accordingly, when we injected OVA-loaded FLT3L-DCs into WT mice, we observed that hyperactive DCs induced the highest frequency and absolute number of SIINFEKL$^+$ CD8$^+$ T cells in the skin dLN, as assessed by H2^{kb}-restricted SIINFEKL (OVA 257–264) tetramer staining (Figures 3A and S3D). The enhanced CD8$^+$ T cell responses mediated by hyperactive DCs were dependent on inflammasomes, since the injection of *Nlrp3*$^{-/-}$ DCs treated with LPS plus PGPC induced weak OVA-specific CD8$^+$ T cell responses (Figures 3A and S3D). Similar weak T cell responses were observed upon injection of *Ccr7*$^{-/-}$ hyperactive DCs (Figures 3A and S3D). These data indicate that hyperactive DCs enhance the generation of antigen-specific CD8$^+$ T cell responses in an inflammasome- and CCR7-dependent manner. In accordance with these data, CD8$^+$ T cells sorted from the dLN displayed the highest frequency of IFNγ expression when isolated from mice that received hyperactive DCs (Figure S3E). Thus, as compared to stimuli that promote pyroptosis (alum) or DC activation (LPS), hyperactivating stimuli elicit the most robust antigen-specific CD8$^+$ T cell responses examined.

IL-1β promotes the reactivation of pre-committed effector T cells, thereby enhancing their cytokine production (Jain et al., 2018). To assess the effect of the direct interaction between hyperactive DCs and effector CD8$^+$ T cells, we performed co-culture assays using differentially stimulated FLT3L-DCs that were also loaded with OVA protein. These DCs were exposed to OVA-specific CD8$^+$ T cells that were sorted from the spleen of mice previously immunized s.c. with OVA antigen emulsified in

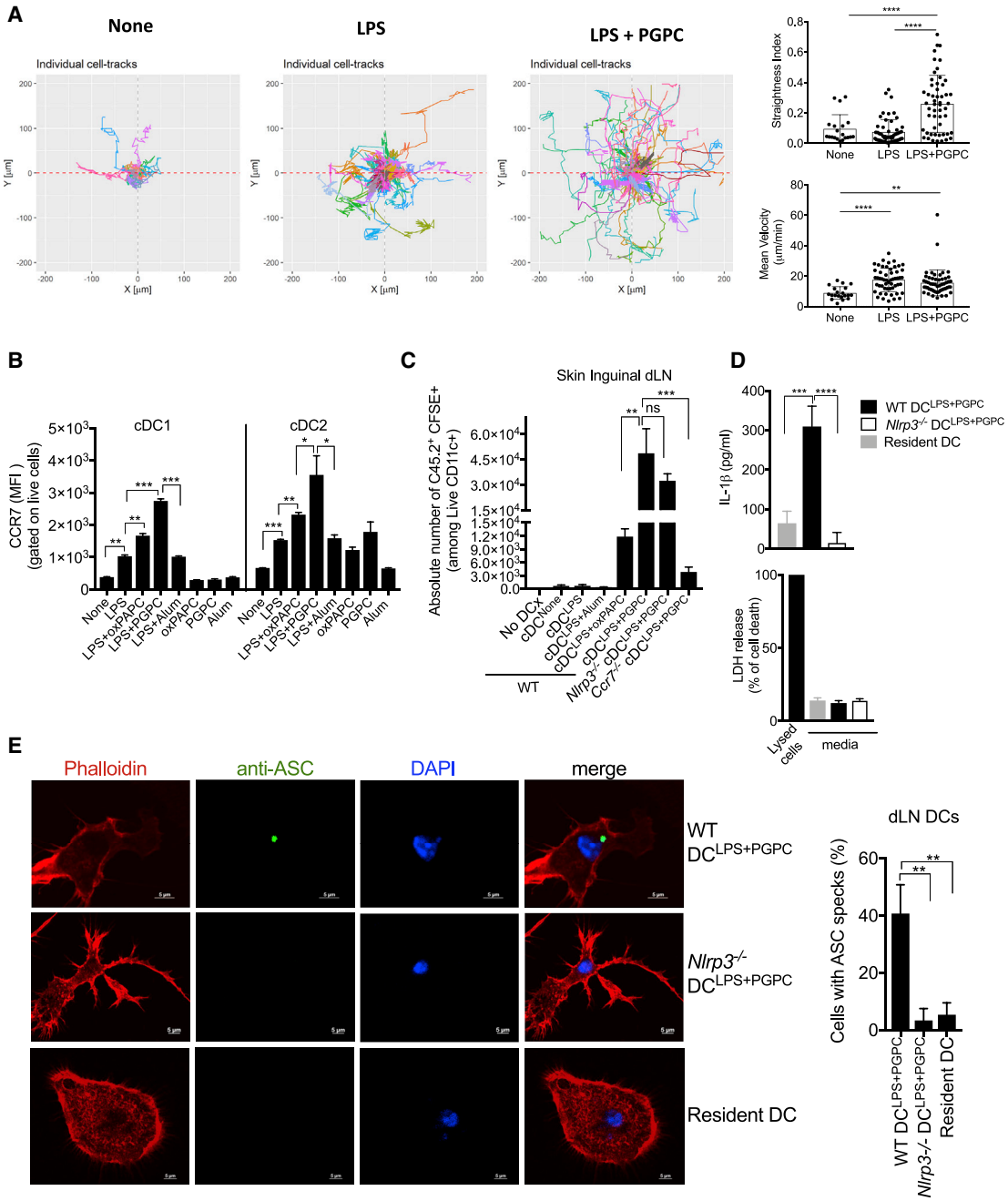

Figure 2. Hyperactive cDCs Display a Hypermigratory Phenotype

(A) FLT3L-derived BMDCs were either left untreated or treated with indicated stimuli. Spider plots depict individual cell trajectories from an origin point (0;0) from four regions of interest. Each trajectory line represents one cell (n = 30–50 cells). Straightness index and mean velocity were calculated (right panels).

(B) cDC1s or cDC2s were either left untreated or treated as indicated. The mean fluorescence intensity (MFI) of surface CCR7 (among CD11c$^+$ live cells) was measured by flow cytometry. Means and SDs from three replicates are shown, and data are representative of at least three independent experiments.

(C) The absolute number of CD45.2$^+$ CFSE$^+$ among CD11c$^+$ live cells was calculated by flow cytometry. Means and SDs from five mice are shown, and data are representative of at least three independent experiments.

(D and E) Hyperactive DCs that migrated to the skin dLN were sorted as CD11c$^+$ CD45.2$^+$ CFSE$^+$ live cells. Alternatively, resident myeloid cells from the skin dLN were sorted as CD11c$^+$ CD45.1$^+$ CFSE^{neg} live cells. (D) Cells were cultured in media for 24 h, and IL-1β and LDH release were measured. Means and SDs from three independent experiments are shown. (E) DCs were stained with the markers indicated and examined by confocal microscopy. Scale bar: 5 µm on representative images (left panel). Quantification of the percent of cells containing ASC specks (right panel). DCx: DC injection.

In (C)–(E), BMDCs were either left untreated or treated with the stimuli indicated. Cells were stained with CFSE and injected subcutaneously into CD45.1 mice. At 15–18 h post-DC injection, skin dLNs were dissected. p values of < 0.05 (*), < 0.01 (**), < 0.001 (***), or ≤ 0.0001 (****) are indicated.

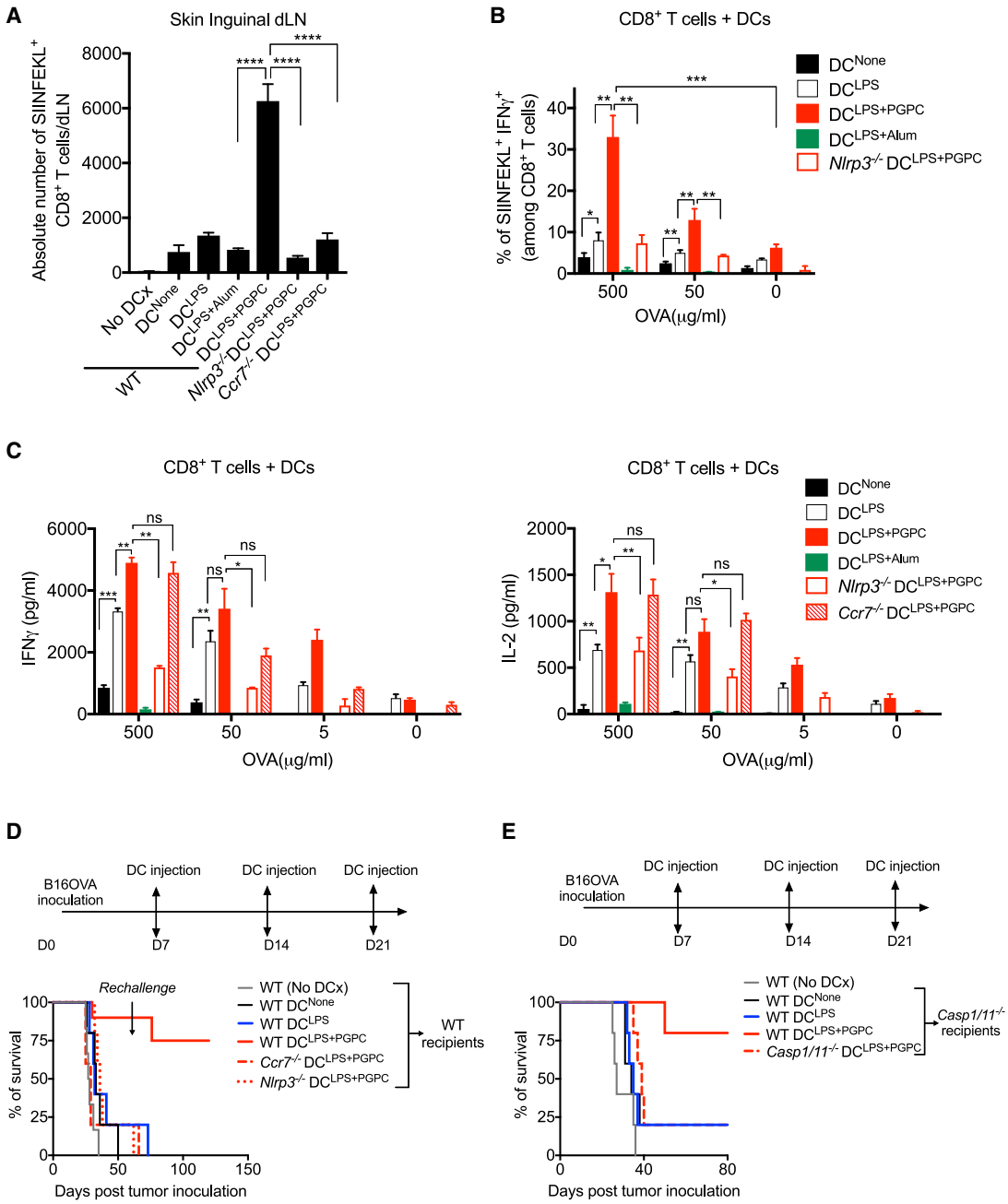

Figure 3. Hyperactive DCs Potentiate CTL Responses in an Inflammasome-Dependent Manner

(A) FLT3L-DCs were either left untreated (DC^{None}) or treated as indicated. 1 × 10e^6 live BMDCs were incubated with OVA protein and injected s.c. into mice. Seven days post-DC injection, the absolute number of $SIINFEKL^+$ $CD8^+$ T cells in the skin dLN was measured by flow cytometry. Means and SDs of five mice are shown.

(B and C) WT mice were immunized with OVA protein. Seven days post-immunization, total $CD8^+$ T cells were isolated from the spleen and co-cultured at a ratio of 10:1 with DCs pretreated with indicated stimuli. DCs were loaded with a serial dilution of OVA protein prior to co-culture. Five days post-coculture, supernatants were collected, and cells were stimulated with phorbol 12-myristate 13-acetate (PMA) and ionomycin in the presence of monensin for intracellular IFNγ staining. (B) The percentage of $SIINFEKL^+$ IFNγ+ T cells was measured by flow cytometry. (C) IFNγ and IL-2 secretion was measured by ELISA. Means and SDs from three replicates are shown, and data are representative of at least two independent experiments.

(D and E) Mice were injected s.c. on the upper right back with 3 × 10^5 of B16OVA cells. Seven days post-tumor cell injection, 1 × 10^6 of FLT3L-DCs of the genotypes indicated were treated as in (A) and incubated with B16OVA WTLs, then injected s.c. on the left flank into tumor-bearing recipient mice. Mice received two subsequent DC injections. The percentage of mice survival was measured (n = 5–6 mice per group, and n = 10 for WT $DC^{LPS+PGPC}$). p values of < 0.05 (*), < 0.01 (**), < 0.001 (***), or ≤ 0.0001 (****) are indicated.

incomplete Freund's adjuvant to generate a resident population of antigen-specific cells. In contrast to naive, active, or pyroptotic DCs, hyperactive DCs strongly stimulated the expansion of OVA-specific $CD8^+$ T cells—as assessed by SIINFEKL tetramer staining—which highly expressed intracellular IFNγ (Figure 3B). Accordingly, total $CD8^+$ T cells produced higher levels of the cytokines IFNγ and IL-2 when co-cultured with hyperactive DCs as compared to naive or active DCs (Figure 3C). Alum-treated pyroptotic DCs failed to stimulate $CD8^+$ T cell effector responses (Figure 3C).

The enhanced ability of hyperactive DCs to stimulate $CD8^+$ T cell effector functions was dependent on inflammasomes, since the co-culture of *Nlrp3*$^{-/-}$ DCs pre-treated with LPS plus PGPC abrogated the enhanced OVA-specific $CD8^+$ T cell responses seen with WT hyperactive DCs (Figures 3B and 3C). Conversely, the ability of hyperactive DCs to stimulate strong $CD8^+$ T cells responses *in vitro* was independent of CCR7, since *Ccr7*$^{-/-}$ hyperactive DCs retain their ability to produce IL-1β from living cells (Figure S3F). As such, *Ccr7*$^{-/-}$ hyperactive DCs also induced $CD8^+$ T cells to produce similar levels of IFNγ and IL-2 as WT hyperactive DCs (Figure 3C). Collectively, these data indicate that hyperactive DCs not only enhance *de novo* antigen-specific $CD8^+$ T cell generation *in vivo*, but also have the ability to reactivate and maintain the effector function of pre-committed $CD8^+$ T cells in an inflammasome-dependent manner.

Hyperactive DCs Induce Long-Lived Anti-tumor Immunity in an Inflammasome-Dependent Manner

We reasoned that hyperactivating stimuli may be particularly useful in the context of cancer immunotherapy. We considered the possibility that hyperactive DCs would allow us to bypass the need for neo-antigen identification and permit the use of whole-tumor cell lysates (WTLs) as an antigen source. WTLs provide a spectrum of mutated and aberrantly expressed tumor-specific antigens (TSAs) and enable the generation of a broad repertoire of T cells specific to tumor-associated antigens.

To determine if conditions that hyperactivate DCs are sufficient to confer anti-tumor immunity, we performed an adoptive transfer of FLT3L-DCs into mice harboring OVA-expressing B16 tumors (B16OVA). To this end, tumor-bearing mice received s.c. injections with differentially stimulated DCs that were loaded with B16OVA WTLs. Hyperactive DCs induced a complete rejection of B16OVA tumors in 90% of tumor-bearing mice (Figure 3D), and 75% of survivor mice rejected a lethal re-challenge with B16OVA cells, which remained tumor-free for more than 100 days post-tumor inoculation (Figure 3D). DCs that were activated with LPS alone and pulsed with B16OVA WTLs provided minimal protection from B16OVA-induced lethality.

The anti-tumor activity of hyperactive DCs was dependent on inflammasomes in these cells, as *Nlrp3*$^{-/-}$ FLT3L-DCs that were treated with WTLs, LPS plus PGPC minimally impacted survival rate (Figure 3D). Hyperactive DC entry to the dLN was crucial for anti-tumor protection, since *Ccr7*$^{-/-}$ DCs treated with WTLs, LPS plus PGPC did not induce tumor rejection (Figure 3D). To further confirm the role of intrinsic inflammasome activation in hyperactive DCs for anti-tumor immune induction, B16OVA tumor-bearing *Casp1/11*$^{-/-}$ mice were injected with either WT-naive, active, or hyperactive DCs loaded with WTLs. We found that naive or active DCs induced a minor tumor rejection in *Casp1/11*$^{-/-}$ mice. In contrast, WT hyperactive DCs induced tumor rejection in ~75% of *Casp1/11*$^{-/-}$ tumor-bearing mice (Figure 3E). This protection was abolished when *Casp1/11*$^{-/-}$ DCs treated with WTLs, LPS plus PGPC were injected into *Casp1/11*$^{-/-}$ tumor-bearing mice. The same trends were observed when injecting WT or *Nlrp3*$^{-/-}$ DCs treated with WTLs, LPS plus PGPC into *Nlrp3*$^{-/-}$-deficient tumor-bearing mice (Figure S3G). These data indicate that hyperactive DCs are sufficient to establish durable anti-tumor immunity and confirm that DC migration into the dLN and inflammasomes within DCs are essential for the anti-tumor activity of hyperactive DCs.

Hyperactivating Stimuli Enhance Memory T Cell Generation and Potentiate Antigen-Specific IFNγ Responses in an Inflammasome-Dependent Manner

We examined if hyperactivating stimuli have a pro-inflammatory effect on endogenous DCs *in vivo*. To test this possibility, mice were immunized s.c. with OVA alone, OVA plus an activating stimulus (LPS), or OVA plus a hyperactivating stimulus (LPS plus oxPAPC or PGPC). Seven and 40 days post-immunization, T effector (Teff), Teff memory (TEM), and T central memory (TCM) cell generation in the dLN was assessed (Sallusto et al., 1999). Seven days post-immunization, hyperactivating stimuli were found to be superior to activating stimuli at inducing $CD8^+$ Teff cells (Figures 4A, upper panel, S4A, and S4B). At this time point, hyperactivating stimuli also induced the highest abundance of $CD8^+$ TEM (Figures 4A, middle panels, S4A, and S4B). Forty days post-immunization, ample TCM cells were observed in mice exposed to hyperactivating stimuli, whereas these cells were less abundant in mice immunized with OVA alone or with LPS (Figure 4A, lower panels). Teff cells were conversely more abundant in mice immunized with OVA plus LPS, as compared to mice immunized with OVA plus oxPAPC or PGPC 40 days post-immunization. These data indicate that hyperactivating stimuli enhance the magnitude and rate of effector and memory T cell generation. When total $CD8^+$ T cells were isolated from mice immunized with hyperactivating stimuli and co-cultured with B16OVA cells, $CD8^+$ T cells exhibited enhanced degranulation activity as compared with T cells that were isolated from mice immunized with OVA alone or OVA plus LPS (Figure 4B). Furthermore, the increase in the frequency of Teff cells 7 days post-immunization correlated with the enhanced IFNγ responses of $CD8^+$ T cells that were isolated from the dLN of mice immunized with OVA plus hyperactivating stimuli (Figure 4C). These results indicate that hyperactivating stimuli potentiate CTL effector functions.

To assess the antigen specificity of individual T cells that result from a s.c. immunization with distinct activation stimuli, mice were injected as described above. Seven days post-immunization, $CD8^+$ T cells were isolated from the skin dLN and re-stimulated *ex vivo* with naive BMDCs loaded with OVA. We found that OVA with hyperactivating stimuli generated the highest frequency of SIINFEKL tetramer$^+$ IFNγ$^+$ responses upon $CD8^+$ T cell re-stimulation with OVA (Figure S4C). NLRP3 activity was required for the hyperactivation-induced enhancement of antigen-specific responses by $CD8^+$ T cells (Figure S4C).

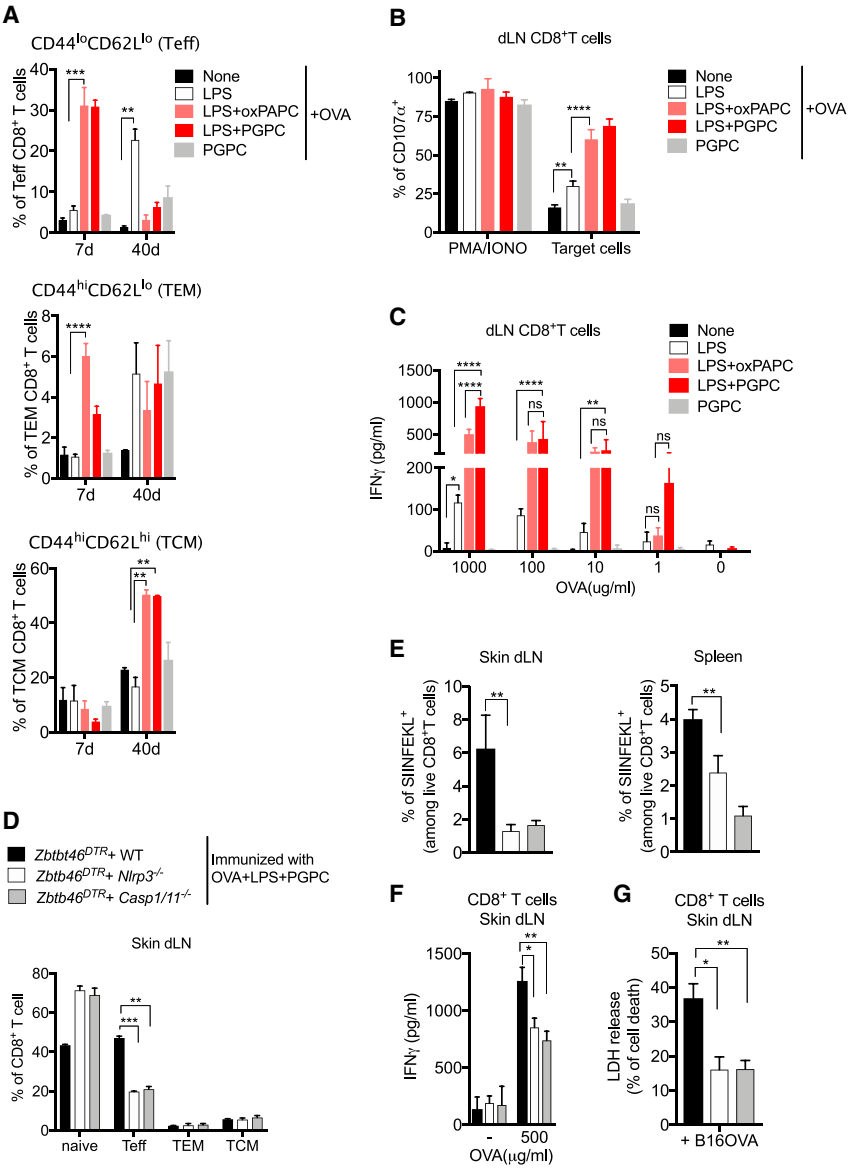

Figure 4. Hyperactivating Stimuli Induce Robust CTL Responses

(A) Mice were injected s.c. on the right flank with OVA either alone or as indicated. Seven or 40 days post-immunization, T cells were isolated from the dLN. (A) The percentage of Teff cells as $CD44^{low}CD62L^{low}$, TEM cells as $CD44^{hi}CD62L^{low}$, and TCM cells as $CD44^{hi}CD62L^{hi}$ are represented among $CD3^+$ $CD8^+$ live cells.

(B and C) $CD8^+$ T cells were sorted from the dLN 7 days post-immunization, then (B) treated either with PMA plus ionomycin, or co-cultured with B16OVA cells (target cells). $CD8^+$ T cells degranulation was assessed by monitoring the percentage of $CD107a^+$. (C) $CD8^+$ T cells were cultured with BMDC loaded (or not) with a serial dilution of OVA protein starting from 1000 μg/ml. IFNγ secretion was measured by ELISA. Means and SDs of five mice are shown.

(D) Seven days post-immunization, the percentage of Teff, TEM, TCM, and T naive cells in the skin dLN was measured by flow cytometry.

(E) The percentage of $SIINFEKL^+$ among $CD8^+$ live T cells in the dLN (left panel) or in the spleen (right panel) was measured by flow cytometry.

(F and G) Total $CD8^+$ T cells were sorted from the dLN and (F) co-cultured with untreated BMDCs loaded (or not) with OVA for 7 days at a ratio of 1:10 (DC: T cell). IFNγ secretion was measured by ELISA. (G) $CD8^+$ T cells were co-cultured with B16OVA cells (target cells) at ratio of 1:3 (effector: target). The percentage of LDH release was measured from B16OVA-$CD8^+$ T cells co-culture and normalized to the LDH released from B16OVA cells or $CD8^+$ T cells cultured separately. Means and SDs from five mice are shown.

In (D)–(F), CD45.1 mice were irradiated then reconstituted with mixed BM of the genotypes indicated. Six weeks post-reconstitution, chimera mice were injected with DTx 3 times a week for a total of 9 DTx injections. Chimeric mice were then immunized s.c. on the right flank with OVA with LPS plus PGPC. p values of < 0.05 (*), < 0.01 (**), < 0.001 (***), or ≤ 0.0001 (****) are indicated.

Furthermore, pyroptotic stimuli (LPS plus alum) were the weakest inducers of antigen-specific responses (Figure S4C). No significant differences in IFNγ were observed among SIINFEKL-negative T cells between immunizations (Figure S4C). Collectively, these data highlight that hyperactivating stimuli induce strong antigen-specific $CD8^+$ T cell responses.

Inflammasome Activation in DCs Potentiates Antigen-Specific CTL Responses

To determine the role of inflammasome activation in endogenous DCs in mediating hyperactivation-based activities, we generated mixed chimeras in mice as previously described (Zanoni et al., 2013). To this end, CD45.1 mice were irradiated and reconstituted with mixed BM using 80% BM cells isolated from *Zbtb46*^{DTR} mice mixed with 20% BM cells isolated from WT, *Nlrp3*$^{-/-}$, or *Casp1/11*$^{-/-}$ mice from a CD45.2 background (Figure S4D). Six weeks post-reconstitution, the efficacy of reconstitution was above 92% efficiency (Figure S4D). Reconstituted mice were then injected intraperitoneally (i.p.) with diphtheria toxin (DTx) to deplete Zbtb46$^+$ cDCs, giving rise to mice that harbor either WT or inflammasome-deficient (*Nlrp3*$^{-/-}$ or *Casp1/11*$^{-/-}$) DCs. Chimera mice were s.c. immunized with OVA plus LPS plus PGPC. Seven days later, $CD8^+$ T cell responses from the skin dLN were assessed. We found that the abundance of Teff $CD8^+$ T cells was reduced in the chimera mice harboring DCs that cannot become hyperactive (*Nlrp3*$^{-/-}$ and *Casp1/11*$^{-/-}$ chimera mice), as compared to chimera mice harboring WT DCs (Figure 4D). Furthermore, the frequency of $SIINFEKL^+$ $CD8^+$ T cells in the dLN or the spleen was reduced in mice harboring *Nlrp3*$^{-/-}$ and *Casp1/11*$^{-/-}$ DCs (Figures 4E and S4E). $CD8^+$ T cells sorted from chimera mice harboring WT DCs produced the highest amounts of IFNγ (Figure 4F) and

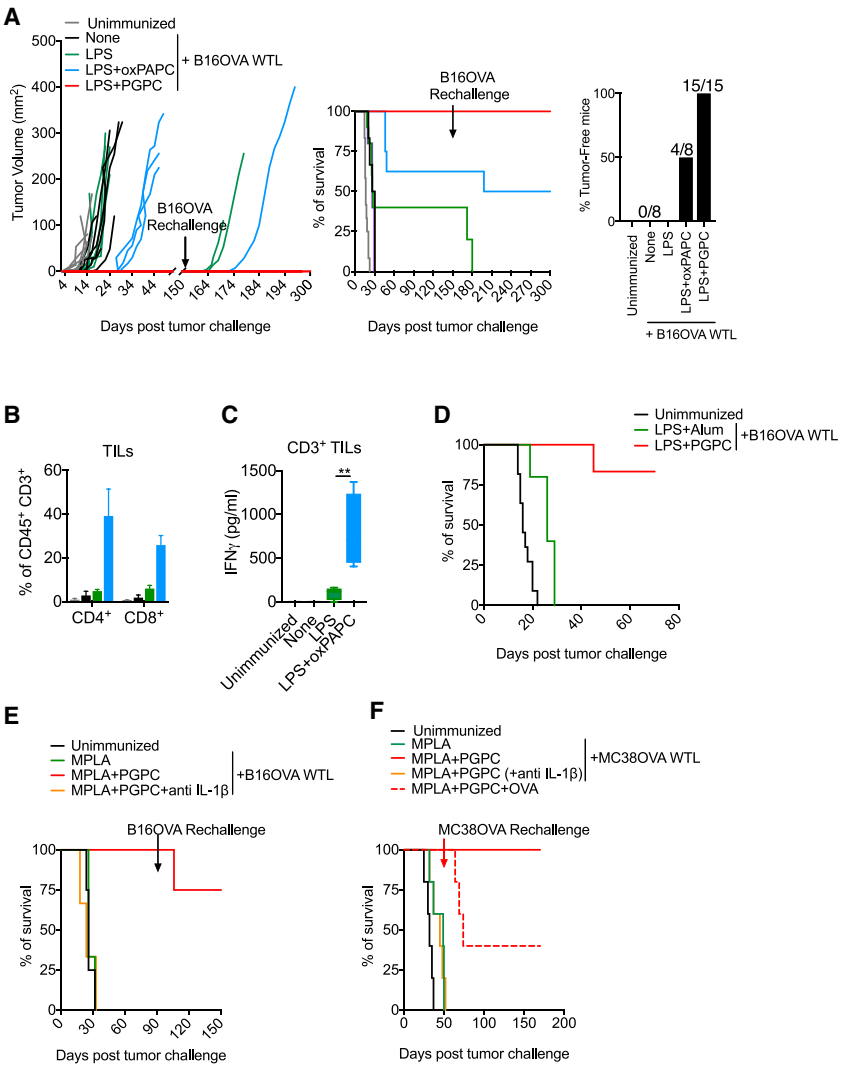

Figure 5. Hyperactivating Stimuli Induce Durable Prophylactic Anti-tumor Immunity in an IL-1β-Dependent Manner

(A) Mice were injected s.c. on the right flank with PBS (unimmunized), with B16OVA cell WTLs alone ("None"), or with LPS, or B16OVA WTLs plus LPS and oxPAPC or PGPC. Fifteen days post-immunization, mice were challenged s.c. on the left upper back with 3×10^5 of B16OVA cells. One hundred fifty days later, tumor-free mice were re-challenged s.c. with 5×10^5 of B16OVA cells. (A) Tumor growth (left panel) and mice survival (middle panel) was monitored every 2 days. The percentage of tumor-free mice 300 days post-tumor inoculation is indicated (right panel) (n = 8–15 mice per group).

(B and C) Tumors were harvested at the endpoint of tumor growth, and (B) the percentages of tumor infiltrating $CD3^+CD4^+$ and $CD3^+CD8^+$ T cells among $CD45^+$ live cells were assessed by flow cytometry. (C) Tumor-infiltrating T cells were sorted then stimulated in the presence of anti-CD3 and anti-CD28 dynabeads. IFNγ release was measured by ELISA (n = 4 mice per group).

(D) Mice were either left untreated (unimmunized) or were immunized s.c. on the right flank with B16OVA WTLs plus the stimuli indicated. Fifteen days post-immunization, mice were challenged with 3×10^5 B16OVA cells s.c. on the left upper back. The percentage of survival is monitored every 2 days (n = 5 mice per group).

(E and F) Mice were either left untreated (unimmunized) or were immunized s.c. on the right flank with B16OVA WTLs (E) or with (F) MC38OVA WTLs or OVA alone or in combination with the treatments indicated. Fifteen days post-immunization, mice were challenged with (E) 3×10^5 of viable B16OVA cells or (F) 5×10^5 MC38OVA cells s.c. on the left upper back. (E) Ninety days later, tumor-free mice were re-challenged with 5×10^5 B16OVA cells s.c. on the back. (F) Fifty days later, tumor-free mice were re-challenged s.c. with 1×10^6 MC38OVA cells. Survival was monitored every 2 days (n = 3–5 mice per group). p values of < 0.01 (**) is indicated.

exhibited higher CTL ability, as compared to $CD8^+$ T cells from mice lacking inflammasome-competent DCs (Figure 4G). In summary, these data demonstrate that (1) endogenous DCs can achieve a state of hyperactivation *in vivo* and potentiate CTL responses, and (2) inflammasomes within endogenous DCs are crucial for hyperactivation-mediated CTL responses.

Hyperactivating Stimuli Stimulate T Cell Responses That Confer Long-Term Anti-tumor Immunity

To address the possibility that hyperactivating stimuli can adjuvant WTLs and mediate strong CTL responses *in vivo*, mice were immunized on the right flank with WTLs alone, WTLs mixed with the activating stimulus LPS, or the hyperactivating stimuli LPS plus oxPAPC or LPS plus PGPC. The source of the WTLs was B16OVA cells. Fifteen days post-immunization, mice were challenged s.c on the left upper back with the parental B16OVA cells. Unimmunized mice or mice immunized with WTLs alone did not exhibit any protection, and all mice succumbed to tumor growth (Figure 5A). Similarly, WTLs plus LPS immunizations offered minimal protection (Figure 5A). In contrast, WTL immunizations in the presence of LPS plus oxPAPC induced a delay in the tumor growth and resulted in a strong protection against subsequent lethal re-challenge with parental B16OVA tumor cells (Figure 5A). Tumors from mice immunized with LPS plus oxPAPC contained a large abundance of $CD4^+$ and $CD8^+$ T cells, as compared to LPS immunizations (Figure 5B). Moreover, when equal numbers of T cells from these tumors were stimulated *ex vivo* with anti-CD3 and anti-CD28, oxPAPC-based immunizations resulted in intra-tumoral T cells that secreted the highest amounts of IFNγ (Figure 5C). Thus, the superior restriction of tumor growth induced by hyperactivating stimuli coincided with inflammatory T cell infiltration into the tumor.

Notably, the protective phenotypes of oxPAPC were superseded by those elicited by PGPC. WTL immunizations in the presence of LPS plus PGPC led to 100% of mice being tumor-free for 150 days post-tumor challenge. These mice rejected a lethal re-challenge with B16OVA cells and remained tumor-free

300 days post-initial tumor challenge (Figure 5A). Interestingly, not all NLRP3 agonists conferred anti-tumor immunity, as LPS plus alum was unable to adjuvant WTLs to protect against tumor growth (Figure 5D). These findings underscore the importance of hyperactive DCs (not pyroptotic DCs) in the induction of anti-tumor immunity.

Similar findings were made when we replaced LPS with monophosphoryl lipid A (MPLA), an FDA-approved TLR4 ligand (Kundi, 2007; Didierlaurent et al., 2009; Paavonen et al., 2009). All mice immunized with MPLA plus PGPC remained tumor-free for 90 days post-tumor B16OVA challenge, and most mice rejected a lethal re-challenge with parental cells (Figure 5E). Similar results were observed in a colon adenocarcinoma MC38OVA model (Figure 5F). These anti-tumor responses were dependent on IL-1β, since neutralizing IL-1β at the time of immunization abolished the protection of mice against tumor growth (Figures 5E and 5F). Interestingly, WTLs were superior at inducing long-term protective immunity after tumor challenge, as compared to immunizations with OVA (Figure 5F). The inability of single antigens to strongly protect from cancer is consistent with work demonstrating the value of using multiple neo-antigens in cancer vaccines (Castle et al., 2012; Ott et al., 2017).

Among memory T cell subsets, T resident memory (TRM) cells, defined by the expression of CD103 and CD69 (Mami-Chouaib et al., 2018), accumulate at the tumor site in various cancer tissues and correlate with a favorable clinical outcome (Webb et al., 2014; Djenidi et al., 2015; Park et al., 2019). We examined the presence of TRM cells at the tumor injection site, as well as the immunization skin biopsies in the survivor mice that were previously immunized with the hyperactivating stimuli LPS plus PGPC. Two hundred days post-tumor inoculation, $CD8^+$ $CD69^+$ $CD103^+$ TRM cells were enriched at the site of tumor injection but were scarce at the immunization site in all survivor mice (Figures S5A and S5B). WTLs and hyperactivating stimuli may therefore generate TRM cells that control local tumor cell growth. To investigate this possibility, we monitored the cytolytic activity of TRM cells from survivor mice. Circulating memory $CD8^+$ T cells and TRM cells were isolated from the spleen or the skin adipose tissue 200 days post-immunization from survivor mice that previously received hyperactivating stimuli. Cytolytic activity, as assessed by LDH release, was only observed when $CD8^+$ T cells were mixed with B16OVA or B16 cells, whereas no killing of unrelated CT26 cells was observed (Figure S5C), highlighting the antigen-specific nature of hyperactivation-induced T cell responses. To further determine if TRM or circulating memory T cells are sufficient to protect against tumor progression, $CD8^+$ T cells were transferred from survivor mice into naive mice and subsequently challenged with the parental tumor cell line used as the initial immunogen. Transfer of $CD8^+$ TRM or circulating $CD8^+$ T cells from survivor mice into naive recipients conferred protection from a subsequent tumor challenge, with the TRM subset playing a dominant protective role (Figure S5D). Transfer of both T cell subsets from survivor mice into naive mice provided 100% protection of recipient mice from subsequent tumor challenges (Figure S5D). These collective data indicate that PGPC-based hyperactivating stimuli confer protection by inducing strong circulating and resident anti-tumor $CD8^+$ T cell responses.

Hyperactivating Stimuli Protect against Established Tumors That Are Resistant to Anti-PD1 Therapy

To determine if hyperactivating stimuli could be harnessed as a cancer immunotherapy, we examined anti-tumor responses in mice that harbored a growing tumor prior to any treatment. For these studies, rather than using parental *in vitro* cultured tumor cells as an antigen source, *ex vivo* WTLs were generated using syngeneic tumors from unimmunized mice, in which 10-mm harvested tumors were dissociated and then depleted of $CD45^+$ cells. Mice were inoculated s.c. with tumor cells on the left upper back. When tumors reached a size of 3–4 mm, tumor-bearing mice were left untreated (unimmunized) or received an injection on the right flank with *ex vivo* WTLs and LPS plus PGPC. Interestingly, hyperactivation-based therapeutic injections induced durable tumor eradication in a range of tumors, such as B16OVA and B16F10 melanoma models, in MC38OVA and CT26 colon cancer tumor models and in Lewis Lung Carcinoma model (LLC1) (Figures 6A–6E and S6A). The efficacy of the immunotherapy was dependent on IL-1β in all the tested models, since the neutralization of IL-1β abolished protection conferred by hyperactivating stimuli plus *ex vivo* WTLs (Figures 6A–6E and S6A). In addition, $CD8^+$ T cells were crucial for protection against immunogenic tumor models such as B16OVA or MC38OVA tumors, whereas $CD4^+$ and $CD8^+$ T cells were both required for protection against less immunogenic tumors such as CT26, B16F10, and LLC1 (Figures 6A–6E and S6A) (Mosely et al., 2017). Interestingly, hyperactivation-based immunotherapy was as efficient as anti-PD-1 therapy in the immunogenic B16OVA model, but more efficient in tumor models that are insensitive to anti-PD-1 treatment such as CT26, B16F10, and LLC1 (Figures 6A–6E and S6A).

The LLC1 cell line is associated with an absence of tumor-infiltrating CTL (Lechner et al., 2013). To determine if hyperactivating stimuli enhance CTL responses in LLC1 tumors, mice harboring a tumor of 4 mm were immunized as described in Figure 6E. Tumor weight was measured for each mouse (Figure S6A) and dissociated, and immune cells were quantified. When mice were treated with anti-PD-1 antibodies, $CD8^+$ tumor-infiltrating lymphocyte (TIL) abundance was similar to TIL abundance in the tumors of unimmunized mice, which is around 1%–2% of TILs (Figures 6F and S6C). In addition, we detected low levels of $CD8^+$ TRM cells in the tumor microenvironment (TME) of unimmunized mice or in mice treated with anti-PD1 (Figures 6F and S6C). Thus, anti-PD-1 treatment had a minimal effect on enhancing anti-LLC1 $CD8^+$ T cell responses. Interestingly, mice immunized with WTLs and LPS plus PGPC induced a strong increase in the frequency of $CD8^+$ TILs (Figure 6F, left panel), and most of these T cells displayed a TRM phenotype (Figures 6F, middle panel, and S6C). The high abundance of $CD8^+$ TRM cells positively correlated with the ability of $CD45^+$ TILs to secrete IFNγ upon CD3/CD28 stimulation, as compared to anti-PD1 treatment (Figure 6F, right panel), and with a higher tumor rejection rate (Figure 6E). Moreover, hyperactivation-mediated enhanced $CD8^+$ T cell responses were dependent on IL-1β, since the immunization of mice with WTLs and LPS plus PGPC in the presence of neutralizing anti-IL-1β antibodies inhibited tumor rejection (Figure 6E), and CTL responses were abrogated (Figure 6F). Similar to conditions of IL-1β inhibition,

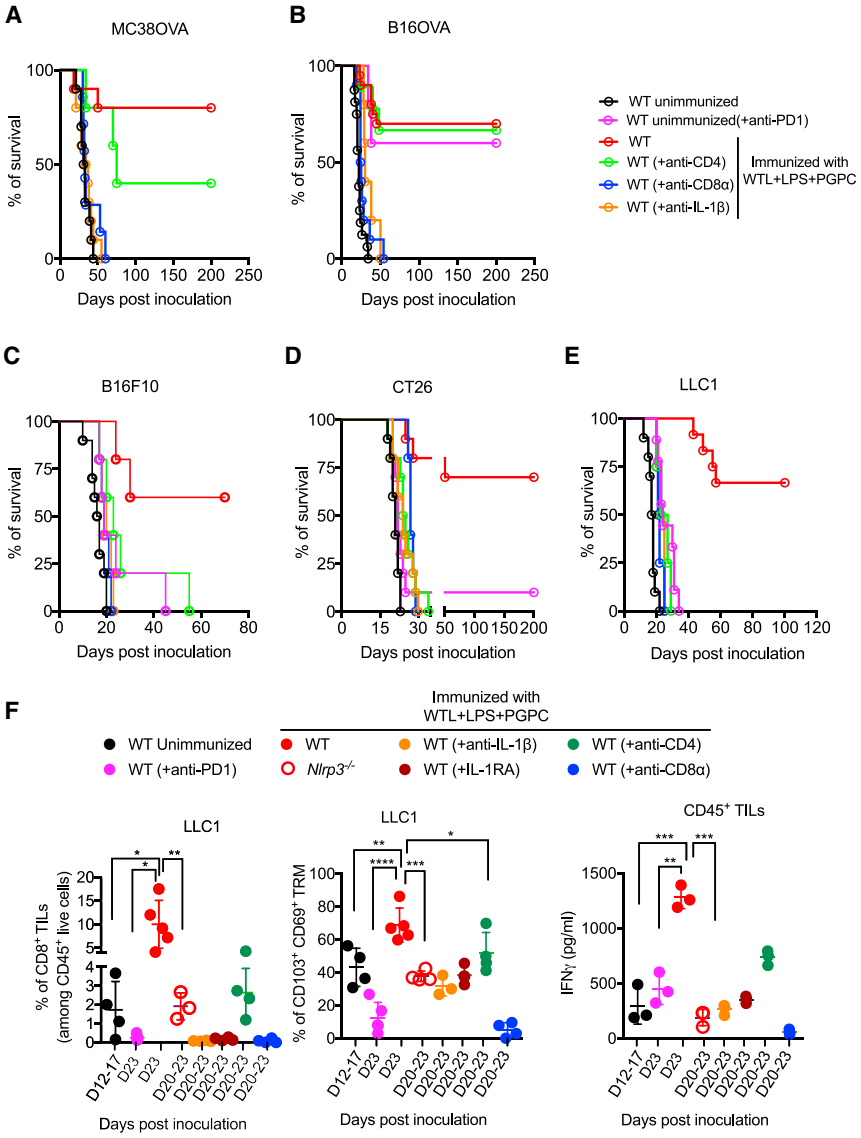

Figure 6. Hyperactivating Stimuli Eradicate Established Tumors That Are Resistant to Checkpoint Inhibitors

Mice of the indicated genotypes were inoculated subcutaneously on the left upper back with (A) 5 × 10^5 of MC38OVA cells, (B) 3 × 10^5 B16OVA cells, (C) 3 × 10^5 B16-F10 cells, (D) 3 × 10^5 CT26 cells, or (E and F) 3 × 10^5 LLC1 cells. In (A)–(E), when tumors reached 3–4 mm in size, mice were either left untreated (unimmunized) or were injected s.c. on the right flank with WTLs plus LPS and PGPC with or without neutralizing anti-IL-1β antibodies, anti-CD4, anti-CD8α antibodies, or (F) IL-RA. Mice received two boost injections with WTLs and LPS plus PGPC. In (B)–(E), alternatively, tumor-bearing mice were injected with anti-PD-1 antibody. The percentage of survival is indicated (n = 10-12 mice per group). In (F), LLC1 tumors were harvested at the endpoint of tumor growth. The percentage of $CD8^+$ TILs (left panel) among $CD3^+CD45^+$ live cells and $CD69^+CD103^+$ TRM cells among $CD8^+$ TILs (middle panel) were measured by flow cytometry. $CD45^+$ live TILs were cultured for 48 h on anti-CD28 and anti-CD3 coated plates. IFNγ was measured by ELISA (right panel) (n = 5 mice per group). p values of < 0.05 (*), < 0.01 (**), < 0.001 (***), or ≤ 0.0001 (****) are indicated.

no protection was conferred to *Nlrp3*$^{-/-}$ or *Casp1/11*$^{-/-}$ mice bearing LLC1 tumors (Figures 6F and S6B). Furthermore, IL-1 signaling was crucial for anti-tumor protection, as IL-1 receptor antagonist (IL-RA) injection abrogated hyperactivation-mediated $CD8^+$ TRM cell infiltration into the tumor (Figures 6F and S6A) and reduced IFNγ-producing T cells in the TME (Figure 6F). As a consequence, in the absence of IL-1β signaling, LLC1 tumor rejection was abrogated (Figures 6E and S6A).

Thus, hyperactivating stimuli strongly potentiate CTL responses in the TME of non-immunogenic tumors in an inflammasome- and IL-1β-dependent manner and induce tumor rejection in models that are resistant to checkpoint immunotherapy.

Hyperactivating Stimuli Protect against Lung Metastasis

We next wondered whether hyperactivation-based immunotherapy can induce distal protection against tumor growth. We used a B16 lung metastasis model in which mice were intravenously (i.v.) injected with B16F10 cells. Seven days post-tumor cells injection, mice were left untreated or received a s.c. immunization with WTL injection alone, WTLs and LPS, or WTLs and LPS plus PGPC. We found that WTL injection alone or in combination with LPS provide some protection against tumor lung colonization in mice. This protection was enhanced when mice received an immunization with WTLs and the hyperactivating stimuli LPS plus PGPC (Figure S6D). These observations indicate that the anti-tumor responses observed can contribute to systemic protection.

Endogenous Hyperactive DCs Stimulate Durable Anti-tumor T Cell Immunity in an Inflammasome-Dependent Manner

To test whether endogenous DCs can initiate hyperactivation-mediated anti-tumor responses, we used *Zbtb46*^{DTR} mice in which cDCs are depleted by DTx injection. When tumors reached 4 mm in size, *Zbtb46*^{DTR} or WT mice were immunized with B16OVA WTLs and LPS plus PGPC. We found that in contrast to WT mice, which rejected tumors in 90% of mice, *Zbtb46*^{DTR} mice, which lack DCs, were unable to reject tumors (Figure 7A). These data confirm that DCs are the initiator of hyperactivation-mediated anti-tumor protection.

We reasoned that inflammasomes within endogenous hyperactive DCs are crucial to mediate long-lived anti-tumor

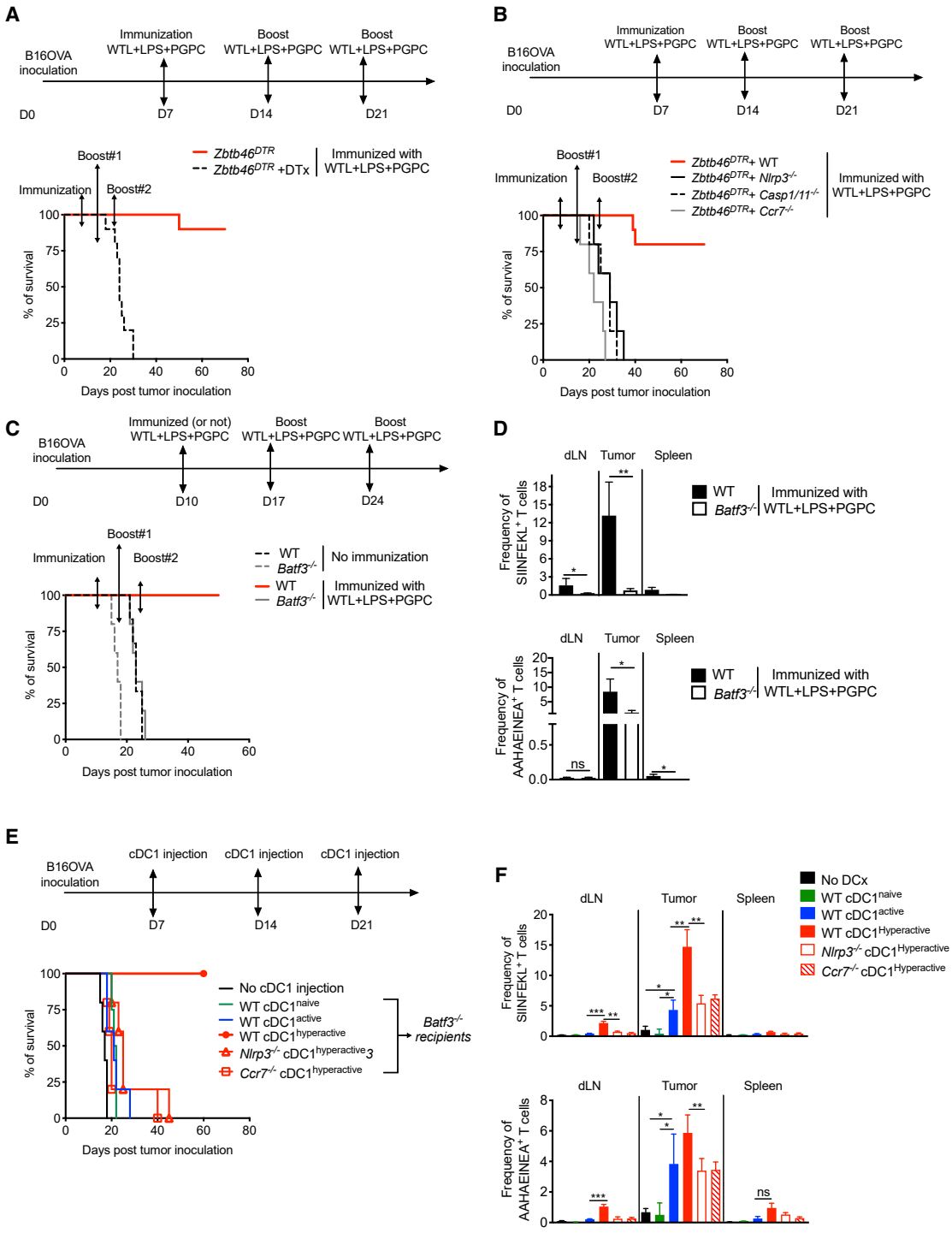

Figure 7. Hyperactive cDC1s Can Use Complex Antigen Sources to Stimulate T-Cell-Mediated Anti-tumor Immunity

(A) *Zbtb46*^{DTR} mice were s.c. injected with B16OVA cells. Mice were either injected with DTx every other day for four consecutive injections, or mice were injected with PBS. Seven days post-tumor injection, all mice were immunized with B16OVA WTLs plus LPS and PGPC, followed by two boost injections. The percentage of mice survival is indicated (n = 10 mice per group).

(B) CD45.1 mice were irradiated then reconstituted with mixed BM from *Zbtb46*^{DTR} mice plus either WT or *Nlrp3*$^{-/-}$, *Casp1/11*$^{-/-}$, or *Ccr7*$^{-/-}$ mice. Six weeks post-reconstitution, mouse chimeras were injected s.c. with B61OVA cells, then all mice received DTx 3 times a week for a total of 12 consecutive injections. Seven days post-tumor inoculation, chimeric mice were immunized with B16OVA WTLs and LPS plus PGPC and received two boost injections. The percentage of mice survival is indicated (n = 5 mice per group).

(legend continued on next page)

immunity. To test this possibility, we generated BM chimeras as described in Figures 4D and S4D. We reconstituted mice with a mix of BM constituted of 80% BM from *Zbtb46*^{DTR} mice and 20% BM from WT mice (in which the DC compartment can be hyperactivated) or 80% BM from *Zbtb46*^{DTR} mice and 20% from inflammasome-deficient *Nlrp3*$^{-/-}$ or *Casp1/11*$^{-/-}$ mice. Chimeric mice were s.c. implanted with B16OVA cells and then injected with DTx to deplete Zbtb46^{+} DCs. When all tumors reached 3 mm in size, mice were immunized with B16OVA WTLs and hyperactivating stimuli LPS plus PGPC. We found that hyperactivating stimuli were effective in inducing tumor rejection only in mice that harbor a WT DC compartment. In contrast, the anti-tumor protection was abrogated in mice harboring inflammasome-deficient DCs (Figure 7B). Similar studies were performed to assess the importance of endogenous hyperactive DC migration. Mixed chimera mice were generated using BM from *Zbtb46*^{DTR} mice and WT or *Ccr7*$^{-/-}$ mice. We found that the ability of DCs to enter the dLN via CCR7 is crucial for DCs to induce tumor rejection, as hyperactivating stimuli were not able to protect mice lacking CCR7 in DCs from tumor progression and lethality (Figures 7B and S7A).

Hyperactive cDC1s Stimulate T-Cell-Mediated Anti-tumor Immunity in an Inflammasome- and CCR7-Dependent Manner

Finally, given the importance of the cDC1 subset in tumor rejection in other experimental contexts, we hypothesized that cDC1s play a central role in inducing hyperactivation-mediated anti-tumor protection. To test this possibility, we used *Batf3*$^{-/-}$ mice (which lack cDC1s) (Hildner et al., 2008). We immunized *Batf3*$^{-/-}$ or WT tumor-bearing mice with LPS plus PGPC and WTLs. WT mice rejected tumors in 100% of mice, whereas all *Batf3*$^{-/-}$ mice succumbed to tumor growth (Figures 7C and S7B). Thus, cDC1s are required for hyperactivation-mediated anti-tumor immunity. In addition, while immunized WT mice induced a high frequency of OVA peptide-specific CD8^{+} and CD4^{+} T cells in the TME and the skin dLN, immunized *Batf3*$^{-/-}$ induced a slightly reduced frequency of antigen-specific CD4^{+} T cells and no antigen-specific CD8^{+} T cells in the TME (Figure 7D).

To further confirm the role of hyperactive cDC1s in anti-tumor protection, we adoptively transferred naive, active, or hyperactive cDC1s into *Batf3*$^{-/-}$ mice. cDC1s were left naive or treated with activating stimuli (LPS) or hyperactivating stimuli (LPS plus PGPC). All cells were loaded with B16OVA WTLs before their s.c. injection into *Batf3*$^{-/-}$ mice that harbored a 3-mm tumor. We found that only hyperactive cDC1s induced tumor rejection in 100% of tumor-bearing mice (Figure 7E). Of note, hyperactive cDC1 injections uniquely restored antigen-specific CD8^{+} T cells in *Batf3*$^{-/-}$ mice in the tumor and the skin dLN (Figures 7F and S7C).

cDC1-mediated tumor rejection was dependent on inflammasomes, since the injection of *Nlrp3*$^{-/-}$ cDC1s that were pre-treated with LPS plus PGPC and loaded with WTLs did not provide any anti-tumor protection and abrogated the ability of hyperactive cDC1s to restore CD8^{+} T cell responses (Figures 7E, 7F, and S7D). Furthermore, cDC1 entry into the dLN played a crucial role in mediating tumor rejection, since the adoptive transfer of *Ccr7*$^{-/-}$ cDC1s that were pre-treated with LPS plus PGPC and loaded with B16OVA WTLs failed to initiate protective anti-tumor immunity (Figures 7E and 7F).

Finally, to address whether the protective immune response is mediated solely by the injected cDC1s or by endogenous DCs capturing the antigen from the injected DCs, we generated full chimeric mice in which the endogenous DC compartment could be depleted prior to cDC1 injection. Six weeks post-reconstitution, mice were s.c. injected with B16OVA cells and subsequently injected with DTx. DTx injection specifically depleted cDCs, whereas the abundance of macrophages was unaffected (Figure S7E). When tumors reached 3–4 mm in all mice, differentially stimulated WT or *Nlrp3*$^{-/-}$ cDC1s that were pre-loaded with B16OVA WTLs were injected. We found that the anti-tumor response was not significantly different between chimeric mice that harbor and do not harbor resident DCs (Figure S7E), indicating that the anti-tumor response generated were primarily mediated by the injected cDC1s . In summary, this study illustrates the importance of hyperactive cDC1s for the establishment of anti-tumor immunity.

DISCUSSION

In this study, we have expanded the immunological activities of hyperactive DCs. Not only are hyperactive DCs capable of releasing IL-1β while maintaining viability, but they also display enhanced migratory capacity to the adjacent dLN via CCR7. Consequently, hyperactive DCs are the most potent stimulators of T cell-mediated immunity that we have examined in mice.

This study also highlights the differences in DC behavior when stimulated with non-pyroptotic inflammasome stimuli versus pyroptotic inflammasome stimuli. It is noteworthy that alum, a well-defined inflammasome stimulus (Kool et al., 2008b), does not exhibit the same activities as PGPC. Indeed, alum induces Th2 immunity (Kool et al., 2008a; Marichal et al., 2011; Oleszycka et al., 2018). One possible reason for the lack of CTL-mediated immunity by alum-treated DCs is based on our findings that alum is a poor inducer of several signals necessary for T cell priming. Consequently, these stimuli are weak inducers

(C and D) WT or *Batf3*$^{-/-}$ mice were injected s.c with B16OVA cells. Seven days post-tumor inoculation, mice were either left untreated, or WT and *Batf3*$^{-/-}$ mice were immunized with B16OVA WTLs and LPS plus PGPC followed by two boost injections. (C) The percentage of mice survival is indicated (n = 10 mice per group). (D) Twenty-one days post-tumor inoculation, the percentage of OVA-specific CD8^{+} T cells and CD4^{+} T cells was assessed using tetramer staining (n = 5 mice per group).

(E and F) *Batf3*$^{-/-}$ mice were injected s.c on the right flank with B16OVA cells. Seven days post-tumor inoculation, mice were left untreated (no cDC1 injection) or were injected s.c. on the left flank with FLT3-derived naive cDC1s or active cDC1s treated with LPS or with hyperactive cDC1s pretreated with LPS plus PGPC. All cDC1s were loaded with B16OVA WTLs for 1 h prior to their injection. (E) The percentage of mice survival is indicated (n = 5 mice per group). (F) Twenty-one days post-tumor inoculation, OVA-specific CD8^{+} T cells and CD4^{+} T cells were assessed using tetramer staining (n = 5 mice per group). p values of < 0.05 (*), < 0.01 (**), or < 0.001 (***) are indicated.

of anti-tumor immunity. In contrast, non-pyroptotic inflammasome activation in DCs induces protective anti-tumor immunity by a process dependent on IL-1 and enhanced cell migration to the dLN. It is likely that each of these activities is important for hyperactive DC functions and contributes to the long-lived T cell-mediated anti-tumor responses. Consistent with this idea, blocking pyroptotic cell death in BMDCs enhances T cell priming (McDaniel et al., 2020), which corroborates our finding that pyroptotic DCs fail to participate in T cell priming and reactivation.

cDC1s were critical for hyperactivation-mediated anti-tumor responses, as hyperactivation-based immunization in *Batf3*$^{-/-}$ mice failed to reject transplanted tumors. This finding is in accordance with studies showing that cDC1s are required for anti-tumor T cell responses in other experimental contexts (Hildner et al., 2008; Ferris et al., 2020). We found that the ability of cDC1s to achieve a hyperactive state increased antigen-specific CD8$^+$ T cell generation, intra-tumoral CTL trafficking, and CTL responses that eradicate many types of tumors. All of these activities were dependent on inflammasomes and the enhanced migratory capacity of hyperactive cDC1s. Consequently, as demonstrated in the LLC1 model, hyperactive cDC1s can convert cold tumors into hot tumors, leading to regression.

Breast cancer patients with a loss-of-function allele of P2X7R, which is essential for activation of the NLRP3 inflammasome and IL-1β secretion, develop a more rapid metastatic disease than individuals bearing the normal allele (Casares et al., 2005; Ghiringhelli et al., 2009). Furthermore, oxaliplatin--treated tumors activate the NLRP3 inflammasome and stimulate IL-1β production, which activates anti-tumor IFNγ-producing CD8$^+$ T cells (Ghiringhelli et al., 2009). If human DCs can achieve a state of hyperactivation, our results may explain why certain chemotherapeutic agents (e.g., oxaliplatin and anthracycline) induce tumor cell death and inflammasome-dependent anti-tumor T cell immunity. Oxaliplatin is a robust stimulator of reactive oxygen species (ROS) production, which can oxidize membranes and create a complex mixture of oxidized lipids that may include PGPC. It is possible that the protective immunity induced by oxaliplatin or ROS inducers results from the actions of hyperactive DCs that prime anti-tumor T cell responses.

We have found that hyperactivating stimuli could be harnessed as an immunotherapy using complex mixtures of antigen. WTL is an attractive source of antigens, as it alleviates the need for neo-antigen identification. Despite the potential benefits offered by WTL-based immunotherapies, prior work in this area has yielded mixed results (Chiang et al., 2015). Our finding that hyperactivating stimuli are capable of adjuvanting WTLs to elicit anti-tumor immunity may explain the lack of success in prior work, as our strategies of DC activation have not previously been considered. On this latter point, it is noteworthy that DC hyperactivating strategies can protect mice from tumors that are sensitive or resistant to PD-1 blockade. The full spectrum of tumors amenable to treatment by hyperactivating stimuli is undefined, but these studies provide a mandate to further explore the value of DC-centric strategies in cancer immunotherapy.

STAR★METHODS

Detailed methods are provided in the online version of this paper and include the following:

- KEY RESOURCES TABLE
- RESOURCE AVAILABILITY
  - Lead Contact
  - Materials Availability
  - Data and Code Availability
- EXPERIMENTAL MODEL AND SUBJECT DETAILS
  - Mouse strains, and Tumor cell lines
  - Differentiation of GM-CSF- and FLT3L-BMDCs
- METHOD DETAILS
  - Generation of full bone marrow chimeric mice for DC injections
  - Generation of full or mixed bone marrow chimeric mice for immunizations
  - Ligand and Chemical Reconstitution
  - DC stimulation and T cell culture
  - LDH Assay and ELISA
  - Antigen uptake and peptide presentation assay
  - DC injections for DC migration assay
  - Microscopy Imaging
  - Cell tracking and time-series analysis
  - Flow cytometry and cell sorting
  - Adoptive DC transfers
  - DC and antigen-specific CD8$^+$ T cell coculture
  - *In vivo* immunization and T cell re-stimulation
  - CD107a degranulation assay
  - *In vitro* cytotoxicity assay
  - Whole tumor lysates preparation
  - Prophylactic immunization and tumor challenges
  - Immunotherapeutic immunization and tumor challenges
  - Tumor infiltrating T cells in the tumor microenvironment
  - *In vivo* immunization and B16-F10 pulmonary colonization
  - Skin biopsies and skin adipose tissue dissociation
  - Adoptive T cell transfer
  - RNA sequencing
- QUANTIFICATION AND STATISTICAL ANALYSIS

SUPPLEMENTAL INFORMATION

Supplemental Information can be found online at https://doi.org/10.1016/j.celrep.2020.108381.

ACKNOWLEDGMENTS

We thank D. Mathis (Harvard), J. Lieberman (Harvard), and N. Joshi (Yale) for advice on this work and the NIH Tetramer Core Facility for providing the OVA peptide tetramers. This work was supported by NIH grants AI133524, AI093589, AI116550, and P30DK34854 and Northwest Bio to J.C.K. D.Z. was supported by the NIH T32 appointments AI007245-34 and AI007245-35. A.K.S. was supported by the Pew-Stewart Scholars Program for Cancer Research, a Sloan Fellowship in Chemistry, and the NIH (1DP2GM119419, 1U54CA217377, and 2RM1HG006193). C.L.S. was supported by K08AI121421, MGH Transformative Scholar Award, and an AAAAI Foundation Faculty Development Award. O.A.C. was supported by T32HL116275. I.Z. is

supported by NIH grants AI121066, DK115217, and AI201700100. J.C.K. and I.Z. hold Investigators in the Pathogenesis of Infectious Disease Awards from the Burroughs Wellcome Fund.

AUTHOR CONTRIBUTIONS

D.Z. designed and performed experiments. D.J.T. consulted on cDC1 and cDC2 differentiations. F.B. and I.Z. designed and generated bone-marrow chimera mice and performed intravenous B16F10 cell injections for metastasis experiments. O.A.C. and C.L.S. generated bone-marrow chimera mice. P.P. analyzed *in vitro* cell tracking data. B.D., I.F., and A.K.S. performed and analyzed RNA sequencing experiments. J.C.K. supervised all research. All authors discussed results and commented on the manuscript.

DECLARATION OF INTERESTS

J.C.K. holds equity and consults for IFM Therapeutics, Quench Bio, and Corner Therapeutics. A.K.S. reports compensation for consulting and/or SAB membership from Merck, Honeycomb Biotechnologies, Cellarity, Repertoire Immune Medicines, Orche Bio, and Dahlia Biosciences. D.Z. holds equity and consults for Corner Therapeutics. Boston Children's Hospital has filed patents related to the use of hyperactivating stimuli and hyperactive DCs in the treatment of disease. J.C.K. serves on the advisory board of *Cell Reports*.

Received: June 29, 2020
Revised: August 19, 2020
Accepted: October 22, 2020
Published: November 17, 2020

REFERENCES

Aglietti, R.A., Estevez, A., Gupta, A., Gonzalez Ramirez, M., Liu, P.S., Kayagaki, N., Ciferri, C., Dixit, V.M., and Dueber, E.C. (2016). GsdmD p30 elicited by caspase-11 during pyroptosis forms pores in membranes. Proc. Natl. Acad. Sci. USA *113*, 7858–7863.

Alvarez, D., Vollmann, E.H., and von Andrian, U.H. (2008). Mechanisms and Consequences of Dendritic Cell Migration. Immunity *29*, 325–342.

Ben-Sasson, S.Z., Hu-Li, J., Quiel, J., Cauchetaux, S., Ratner, M., Shapira, I., Dinarello, C.A., and Paul, W.E. (2009). IL-1 acts directly on CD4 T cells to enhance their antigen-driven expansion and differentiation. Proc. Natl. Acad. Sci. USA *106*, 7119–7124.

Ben-Sasson, S.Z., Hogg, A., Hu-Li, J., Wingfield, P., Chen, X., Crank, M., Caucheteux, S., Ratner-Hurevich, M., Berzofsky, J.A., Nir-Paz, R., and Paul, W.E. (2013). IL-1 enhances expansion, effector function, tissue localization, and memory response of antigen-specific CD8 T cells. J. Exp. Med. *210*, 491–502.

Brubaker, S.W., Bonham, K.S., Zanoni, I., and Kagan, J.C. (2015). Innate immune pattern recognition: a cell biological perspective. Annu. Rev. Immunol. *33*, 257–290.

Cancel, J.-C., Crozat, K., Dalod, M., and Mattiuz, R. (2019). Are Conventional Type 1 Dendritic Cells Critical for Protective Antitumor Immunity and How? Front. Immunol. *10*, 9.

Casares, N., Pequignot, M.O., Tesniere, A., Ghiringhelli, F., Roux, S., Chaput, N., Schmitt, E., Hamai, A., Hervas-Stubbs, S., Obeid, M., et al. (2005). Caspase-dependent immunogenicity of doxorubicin-induced tumor cell death. J. Exp. Med. *202*, 1691–1701.

Castle, J.C., Kreiter, S., Diekmann, J., Löwer, M., van de Roemer, N., de Graaf, J., Selmi, A., Diken, M., Boegel, S., Paret, C., et al. (2012). Exploiting the mutanome for tumor vaccination. Cancer Res. *72*, 1081–1091.

Chen, K.W., Groß, C.J., Sotomayor, F.V., Stacey, K.J., Tschopp, J., Sweet, M.J., and Schroder, K. (2014). The neutrophil NLRC4 inflammasome selectively promotes IL-1β maturation without pyroptosis during acute Salmonella challenge. Cell Rep. *8*, 570–582.

Chiang, C., Coukos, G., and Kandalaft, L. (2015). Whole Tumor Antigen Vaccines: Where Are We? Vaccines *3*, 344–372.

Didierlaurent, A.M., Morel, S., Lockman, L., Giannini, S.L., Bisteau, M., Carlsen, H., Kielland, A., Vosters, O., Vanderheyde, N., Schiavetti, F., et al. (2009). AS04, an aluminum salt- and TLR4 agonist-based adjuvant system, induces a transient localized innate immune response leading to enhanced adaptive immunity. J. Immunol. *183*, 6186–6197.

Djenidi, F., Adam, J., Goubar, A., Durgeau, A., Meurice, G., de Montpréville, V., Validire, P., Besse, B., and Mami-Chouaib, F. (2015). CD8+CD103+ tumor-infiltrating lymphocytes are tumor-specific tissue-resident memory T cells and a prognostic factor for survival in lung cancer patients. J. Immunol. *194*, 3475–3486.

Eisenbarth, S.C., Colegio, O.R., O'Connor, W., Sutterwala, F.S., and Flavell, R.A. (2008). Crucial role for the Nalp3 inflammasome in the immunostimulatory properties of aluminium adjuvants. Nature *453*, 1122–1126.

Evavold, C.L., Ruan, J., Tan, Y., Xia, S., Wu, H., and Kagan, J.C. (2017). The Pore-Forming Protein Gasdermin D Regulates Interleukin-1 Secretion from Living Macrophages. Immunity *48*, 35–44.e6.

Ferris, S.T., Durai, V., Wu, R., Theisen, D.J., Ward, J.P., Bern, M.D., Davidson, J.T., Bagadia, P., Liu, T., Briseño, C.G., et al. (2020). cDC1 prime and are licensed by CD4+ T cells to induce anti-tumour immunity. Nature *584*, 624–629.

Gaidt, M.M., Ebert, T.S., Chauhan, D., Schmidt, T., Schmid-Burgk, J.L., Rapino, F., Robertson, A.A., Cooper, M.A., Graf, T., and Hornung, V. (2016). Human Monocytes Engage an Alternative Inflammasome Pathway. Immunity *44*, 833–846.

Garlanda, C., Dinarello, C.A., and Mantovani, A. (2013). The interleukin-1 family: back to the future. Immunity *39*, 1003–1018.

Ghiringhelli, F., Apetoh, L., Tesniere, A., Aymeric, L., Ma, Y., Ortiz, C., Vermaelen, K., Panaretakis, T., Mignot, G., Ullrich, E., et al. (2009). Activation of the NLRP3 inflammasome in dendritic cells induces IL-1beta-dependent adaptive immunity against tumors. Nat. Med. *15*, 1170–1178.

Hildner, K., Edelson, B.T., Purtha, W.E., Diamond, M., Matsushita, H., Kohyama, M., Calderon, B., Schraml, B.U., Unanue, E.R., Diamond, M.S., et al. (2008). Batf3 deficiency reveals a critical role for CD8α+ dendritic cells in cytotoxic T cell immunity. Science *322*, 1097–1100.

Inaba, K., Turley, S., Iyoda, T., Yamaide, F., Shimoyama, S., Reis e Sousa, C., Germain, R.N., Mellman, I., and Steinman, R.M. (2000). The formation of immunogenic major histocompatibility complex class II-peptide ligands in lysosomal compartments of dendritic cells is regulated by inflammatory stimuli. J. Exp. Med. *191*, 927–936.

Jain, A., Song, R., Wakeland, E.K., and Pasare, C. (2018). T cell-intrinsic IL-1R signaling licenses effector cytokine production by memory CD4 T cells. Nat. Commun. *9*, 3185.

Janeway, C.A., Jr., and Medzhitov, R. (2002). Innate immune recognition. Annu. Rev. Immunol. *20*, 197–216.

Kagan, J.C., Magupalli, V.G., and Wu, H. (2014). SMOCs: supramolecular organizing centres that control innate immunity. Nat. Rev. Immunol. *14*, 821–826.

Kayagaki, N., Stowe, I.B., Lee, B.L., O'Rourke, K., Anderson, K., Warming, S., Cuellar, T., Haley, B., Roose-Girma, M., Phung, Q.T., et al. (2015). Caspase-11 cleaves gasdermin D for non-canonical inflammasome signalling. Nature *526*, 666–671.

Kieser, K.J., and Kagan, J.C. (2017). Multi-receptor detection of individual bacterial products by the innate immune system. Nat. Rev. Immunol. *17*, 376–390.

Kim, D., Langmead, B., and Salzberg, S.L. (2015). HISAT: a fast spliced aligner with low memory requirements. Nat. Methods *12*, 357–360.

Kool, M., Soullié, T., van Nimwegen, M., Willart, M.A., Muskens, F., Jung, S., Hoogsteden, H.C., Hammad, H., and Lambrecht, B.N. (2008a). Alum adjuvant boosts adaptive immunity by inducing uric acid and activating inflammatory dendritic cells. J. Exp. Med. *205*, 869–882.

Kool, M., Pétrilli, V., De Smedt, T., Rolaz, A., Hammad, H., van Nimwegen, M., Bergen, I.M., Castillo, R., Lambrecht, B.N., and Tschopp, J. (2008b). Cutting edge: alum adjuvant stimulates inflammatory dendritic cells through activation of the NALP3 inflammasome. J. Immunol. *181*, 3755–3759.

Kundi, M. (2007). New hepatitis B vaccine formulated with an improved adjuvant system. Expert Rev. Vaccines *6*, 133–140.

Lamkanfi, M., and Dixit, V.M. (2014). Mechanisms and functions of inflammasomes. Cell *157*, 1013–1022.

Lechner, M.G., Karimi, S.S., Barry-Holson, K., Angell, T.E., Murphy, K.A., Church, C.H., Ohlfest, J.R., Hu, P., and Epstein, A.L. (2013). Immunogenicity of murine solid tumor models as a defining feature of in vivo behavior and response to immunotherapy. J. Immunother. *36*, 477–489.

Lee, P.-H., Yamamoto, T.N., Gurusamy, D., Sukumar, M., Yu, Z., Hu-Li, J., Kawabe, T., Gangaplara, A., Kishton, R.J., Henning, A.N., et al. (2019). Host conditioning with IL-1β improves the antitumor function of adoptively transferred T cells. J. Exp. Med. *216*, 2619–2634.

Li, B., and Dewey, C.N. (2011). RSEM: accurate transcript quantification from RNA-Seq data with or without a reference genome. BMC Bioinformatics *12*, 323.

Linkert, M., Rueden, C.T., Allan, C., Burel, J.-M., Moore, W., Patterson, A., Loranger, B., Moore, J., Neves, C., MacDonald, D., et al. (2010). Metadata matters: Access to image data in the real world. J. Cell Biol. *189*, 777–782.

Liu, X., Zhang, Z., Ruan, J., Pan, Y., Magupalli, V.G., Wu, H., and Lieberman, J. (2016). Inflammasome-activated gasdermin D causes pyroptosis by forming membrane pores. Nature *535*, 153–158.

Love, M.I., Huber, W., and Anders, S. (2014). Moderated estimation of fold change and dispersion for RNA-seq data with DESeq2. Genome Biol. *15*, 550.

Lu, A., Magupalli, V.G., Ruan, J., Yin, Q., Atianand, M.K., Vos, M.R., Schröder, G.F., Fitzgerald, K.A., Wu, H., and Egelman, E.H. (2014). Unified polymerization mechanism for the assembly of ASC-dependent inflammasomes. Cell *156*, 1193–1206.

Mami-Chouaib, F., Blanc, C., Corgnac, S., Hans, S., Malenica, I., Granier, C., Tihy, I., and Tartour, E. (2018). Resident memory T cells, critical components in tumor immunology. J. Immunother. Cancer *6*, 87.

Marichal, T., Ohata, K., Bedoret, D., Mesnil, C., Sabatel, C., Kobiyama, K., Lekeux, P., Coban, C., Akira, S., Ishii, K.J., et al. (2011). DNA released from dying host cells mediates aluminum adjuvant activity. Nat. Med. *17*, 996–1002.

Marrack, P., McKee, A.S., and Munks, M.W. (2009). Towards an understanding of the adjuvant action of aluminium. Nat. Rev. Immunol. *9*, 287–293.

MartÍn-Fontecha, A., Sebastiani, S., Höpken, U.E., Uguccioni, M., Lipp, M., Lanzavecchia, A., and Sallusto, F. (2003). Regulation of dendritic cell migration to the draining lymph node: impact on T lymphocyte traffic and priming. J. Exp. Med. *198*, 615–621.

Matzinger, P. (2002). The danger model: a renewed sense of self. Science *296*, 301–305.

McDaniel, M.M., Kottyan, L.C., Singh, H., and Pasare, C. (2020). Suppression of Inflammasome Activation by IRF8 and IRF4 in cDCs Is Critical for T Cell Priming. Cell Rep. *31*, 107604.

Mellman, I., and Steinman, R.M. (2001). Dendritic cells: specialized and regulated antigen processing machines. Cell *106*, 255–258.

Mempel, T.R., Henrickson, S.E., and Von Andrian, U.H. (2004). T-cell priming by dendritic cells in lymph nodes occurs in three distinct phases. Nature *427*, 154–159.

Monteleone, M., Stanley, A.C., Chen, K.W., Brown, D.L., Bezbradica, J.S., von Pein, J.B., Holley, C.L., Boucher, D., Shakespear, M.R., Kapetanovic, R., et al. (2018). Interleukin-1β Maturation Triggers Its Relocation to the Plasma Membrane for Gasdermin-D-Dependent and -Independent Secretion. Cell Rep. *24*, 1425–1433.

Mosely, S.I.S., Prime, J.E., Sainson, R.C.A., Koopmann, J.-O., Wang, D.Y.Q., Greenawalt, D.M., Ahdesmaki, M.J., Leyland, R., Mullins, S., Pacelli, L., et al. (2017). Rational Selection of Syngeneic Preclinical Tumor Models for Immunotherapeutic Drug Discovery. Cancer Immunol. Res. *5*, 29–41.

Ohl, L., Mohaupt, M., Czeloth, N., Hintzen, G., Kiafard, Z., Zwirner, J., Blankenstein, T., Henning, G., and Förster, R. (2004). CCR7 governs skin dendritic cell migration under inflammatory and steady-state conditions. Immunity *21*, 279–288.

Oleszycka, E., McCluskey, S., Sharp, F.A., Munoz-Wolf, N., Hams, E., Gorman, A.L., Fallon, P.G., and Lavelle, E.C. (2018). The vaccine adjuvant alum promotes IL-10 production that suppresses Th1 responses. Eur. J. Immunol. *48*, 705–715.

Ott, P.A., Hu, Z., Keskin, D.B., Shukla, S.A., Sun, J., Bozym, D.J., Zhang, W., Luoma, A., Giobbie-Hurder, A., Peter, L., et al. (2017). An immunogenic personal neoantigen vaccine for patients with melanoma. Nature *547*, 217–221.

Paavonen, J., Naud, P., Salmerón, J., Wheeler, C.M., Chow, S.N., Apter, D., Kitchener, H., Castellsague, X., Teixeira, J.C., Skinner, S.R., et al.; HPV PATRICIA Study Group (2009). Efficacy of human papillomavirus (HPV)-16/18 AS04-adjuvanted vaccine against cervical infection and precancer caused by oncogenic HPV types (PATRICIA): final analysis of a double-blind, randomised study in young women. Lancet *374*, 301–314.

Park, S.L., Buzzai, A., Rautela, J., Hor, J.L., Hochheiser, K., Effern, M., McBain, N., Wagner, T., Edwards, J., McConville, R., et al. (2019). Tissue-resident memory $CD8^+$ T cells promote melanoma-immune equilibrium in skin. Nature *565*, 366–371.

Picelli, S., Faridani, O.R., Björklund, A.K., Winberg, G., Sagasser, S., and Sandberg, R. (2014). Full-length RNA-seq from single cells using Smart-seq2. Nat. Protoc. *9*, 171–181.

Sabado, R.L., Balan, S., and Bhardwaj, N. (2017). Dendritic cell-based immunotherapy. Cell Res. *27*, 74–95.

Sallusto, F., Lenig, D., Förster, R., Lipp, M., and Lanzavecchia, A. (1999). Two subsets of memory T lymphocytes with distinct homing potentials and effector functions. Nature *401*, 708–712.

Schindelin, J., Arganda-Carreras, I., Frise, E., Kaynig, V., Longair, M., Pietzsch, T., Preibisch, S., Rueden, C., Saalfeld, S., Schmid, B., et al. (2012). Fiji: an open-source platform for biological-image analysis. Nat. Methods *9*, 676–682.

Stuart, T., Butler, A., Hoffman, P., Hafemeister, C., Papalexi, E., Mauck, W.M., 3rd, Hao, Y., Stoeckius, M., Smibert, P., and Satija, R. (2019). Comprehensive Integration of Single-Cell Data. Cell *177*, 1888–1902.e21.

Theisen, D.J., Ferris, S.T., Briseño, C.G., Kretzer, N., Iwata, A., Murphy, K.M., and Murphy, T.L. (2019). *Batf3*-Dependent Genes Control Tumor Rejection Induced by Dendritic Cells Independently of Cross-Presentation. Cancer Immunol. Res. *7*, 29–39.

Tzeng, T.C., Schattgen, S., Monks, B., Wang, D., Cerny, A., Latz, E., Fitzgerald, K., and Golenbock, D.T. (2016). A Fluorescent Reporter Mouse for Inflammasome Assembly Demonstrates an Important Role for Cell-Bound and Free ASC Specks during In Vivo Infection. Cell Rep. *16*, 571–582.

Webb, J.R., Milne, K., Watson, P., Deleeuw, R.J., and Nelson, B.H. (2014). Tumor-infiltrating lymphocytes expressing the tissue resident memory marker CD103 are associated with increased survival in high-grade serous ovarian cancer. Clin. Cancer Res. *20*, 434–444.

Wolf, A.J., Reyes, C.N., Liang, W., Becker, C., Shimada, K., Wheeler, M.L., Cho, H.C., Popescu, N.I., Coggeshall, K.M., Arditi, M., and Underhill, D.M. (2016). Hexokinase Is an Innate Immune Receptor for the Detection of Bacterial Peptidoglycan. Cell *166*, 624–636.

Zanoni, I., Spreafico, R., Bodio, C., Di Gioia, M., Cigni, C., Broggi, A., Gorletta, T., Caccia, M., Chirico, G., Sironi, L., et al. (2013). IL-15 cis presentation is required for optimal NK cell activation in lipopolysaccharide-mediated inflammatory conditions. Cell Rep. *4*, 1235–1249.

Zanoni, I., Tan, Y., Di Gioia, M., Broggi, A., Ruan, J., Shi, J., Donado, C.A., Shao, F., Wu, H., Springstead, J.R., and Kagan, J.C. (2016). An endogenous caspase-11 ligand elicits interleukin-1 release from living dendritic cells. Science *352*, 1232–1236.

Zanoni, I., Tan, Y., Di Gioia, M., Springstead, J.R., and Kagan, J.C. (2017). By Capturing Inflammatory Lipids Released from Dying Cells, the Receptor CD14 Induces Inflammasome-Dependent Phagocyte Hyperactivation. Immunity *47*, 697–709.e3.

STAR★METHODS

KEY RESOURCES TABLE

REAGENT or RESOURCE	SOURCE	IDENTIFIER
Antibodies		
PE/Cyanine7 anti-mouse CD11c Antibody (clone N418)	BioLegend	117318
PerCP anti-mouse I-A/I-E Antibody (clone M5/114.15.2)	BioLegend	107624
APC anti-mouse CD40 Antibody (clone3/23)	BioLegend	124612
FITC anti-mouse CD80 Antibody (clone 16-10A1)	BioLegend	104706
PE anti-mouse CD69 Antibody (clone H1.2F3)	BioLegend	104508
APC anti-mouse H-2Kb Antibody (clone AF6-88.5)	BioLegend	116518
PE anti-mouse CD197 (CCR7) Antibody (clone 4B12)	BioLegend	120106
PerCP-eFluor 710 anti-mouse SIRP alpha Antibody (clone P84)	BD Biosciences	46-1721-82
PE/Cy7 anti-mouse CD24 Antibody (clone M1/69)	BioLegend	101822
APC-eFluor 780 anti-mouse CD11c Antibody (clone N418)	ThermoFisher	47-0114-82
VioletFluor 450 anti-Mouse MHC Class II (clone M5/114.15.2)	VWR	75-5321-U100
Alexa Fluor® 488 Rat Anti-Mouse CD45R (clone RA3-6B2)	BD Biosciences	557669
Alexa Fluor® 647 anti-Mouse CD64 a and b Alloantigens (clone X54-5/7.1)	BD Biosciences	558539
PE anti-mouse F4/80 Antibody (clone BM8)	ThermoFisher	12-4801-82
PerCP/Cy5.5 anti-mouse CD45.1 Antibody (clone A20)	BioLegend	110728
APC anti-mouse CD45.2 Antibody (clone 104)	BioLegend	109814
APC anti-mouse CD8a Antibody (clone 53–6.7)	BioLegend	100712
PerCP/Cyanine5.5 anti-mouse CD107a (LAMP-1) Antibody	BioLegend	121626
Brilliant Violet 510 anti-mouse CD4 Antibody (clone RM4-5)	BioLegend	100559
PE/Cyanine7 anti-mouse/human CD44 Antibody (clone IM7)	BioLegend	103030
Alexa Fluor® 488 anti-mouse CD62L Antibody (clone MEL-14)	BioLegend	104420
PerCP/Cyanine5.5 anti-mouse CD3 Antibody (clone 17A2)	BioLegend	100218
Alexa Fluor® 647 anti-mouse CD103 Antibody (clone 2E7)	BioLegend	121410
PE anti-mouse CD69 Antibody (clone H1.2F3)	BioLegend	104508
Brilliant Violet 711 anti-mouse CD45 Antibody (clone 30F11)	BioLegend	103147
Alexa Fluor® 488 anti-mouse IFNγ Antibody (clone XMG1.2)	BioLegend	505813
PE-conjugated H2K(b) SIINFEKL (OVA 257-264)	NIH Tetramer Core Facility	N/A
APC conjugated I-A(b) AAHAEINEA (OVA 329-337)	NIH Tetramer Core Facility	N/A
I-A(b) and H2K(b) associated with CLIP peptides PVSKMRMATPLLMQA	NIH Tetramer Core Facility	N/A
FITC anti-mouse CD8.1, Lyt-2.1 (clone CD8-E1)	Accurate Chemicals	DEV102-1-4/02
APC anti-mouse H-2Kb Antibody (Clone AF6-88.5)	BioLegend	116518
PE anti-mouse H-2Kb bound to SIINFEKL Antibody (Clone 25-D1.16)	BioLegend	141604
Ultra-LEAF Purified anti-mouse CD8a Antibody (clone 53-6.7)	BioLegend	100746
Ultra-LEAF Purified anti-mouse CD4 Antibody (clone GK1.5)	BioLegend	100442
LEAF Purified anti-mouse / rat IL-1β Antibody	BioLegend	503504
Ultra-LEAF Purified anti-mouse CD279 (PD-1) (clone 29F.1A12)	BioLegend	135247
IL-1R Antagonist	Cayman Chemical	21349
PerCP/Cyanine5.5 anti-mouse TCR β chain Antibody	BioLegend	109228
anti-Asc, pAb (AL177)	Adipogen	Cat# AG-25B-0006; RRID: AB_2490440
Chicken anti-Rabbit IgG Secondary Antibody, AF488	Thermo Fisher	A-21441
Alexa Fluor 647 Phalloidin	Thermo Fisher	A22287
Phalloidin-iFluor 488	Abcam	ab176753

(*Continued on next page*)

Continued

REAGENT or RESOURCE	SOURCE	IDENTIFIER
Chemicals, Peptides, and Recombinant Proteins		
E. coli LPS Serotype O55:B5-TLR grade	Enzo Life Sciences	ALX-581-013-L001
PGPC	Cayman Chemical	10044
Monophosphoryl Lipid A (MPLA)	Invivogen	tlrl-mpla
oxPAPC	Invivogen	tlrl-oxp1
CpG ODN 1826	Invivogen	tlrl-1826-1
Incomplete Freund's Adjuvant	Sigma Aldrich	F550
Alhydrogel	Invivogen	vac-alu-250
Addavax MF-59	Invivogen	vac-adx-10
phorbol 12-myristate 13-acetate (PMA) and ionomycin	Biolegend	423301
Brefeldin A Solution (1,000X)	Biolegend	420601
Dynabeads Mouse T-Activator CD3/CD28	ThermoFisher	11456D
Ovalbumin, Alexa Fluor 488 Conjugate	ThermoFisher	O34781
EndoFit Ovalbumin	Invivogen	vac-pova
Dextran, Alexa Fluor 488; 10,000 MW	ThermoFisher	D22910
Recombinant Murine IL-2	Peprotech	212-12
Critical Commercial Assays		
Mouse IL-1b ELISA Kit	Thermofisher	88-7013-86
Mouse TNFa ELISA Kit	Thermofisher	88-7324-88
Mouse IFN gamma ELISA Kit	Thermofisher	88-7314-77
Mouse IL-2 ELISA Kit	Thermofisher	88-7024-88
CyQUANT LDH Cytotoxicity Assay	Thermofisher	C20300
CD45 (TIL) MicroBeads, mouse	Miltenyi Biotec	130-110-618
Tumor Dissociation Kit, mouse	Miltenyi Biotec	130-096-730
CD8a (Ly-2) MicroBeads, mouse	Miltenyi Biotec	130-117-044
CD4 (L3T4) MicroBeads, mouse	Miltenyi Biotec	130-117-043
LIVE/DEAD Violet Viability Kit	Thermofisher	L34958
CellTrace CFSE Cell Proliferation Kit	Thermofisher	C34554
BD Cytofix/Cytoperm	BD Biosciences	554714
RNeasy Plus Micro Kit	QIAGEN	74034
Deposited Data		
Expression profiling by high throughput RNA sequencing	GEO accession numbers	GSE156159
Experimental Models: Cell Lines		
B16.F10 cell line	Arlene Sharpe Laboratory	N/A
B16.F10 OVA cell line	Arlene Sharpe Laboratory	N/A
MC-38 OVA cell line	Arlene Sharpe Laboratory	N/A
CT26 cell line	Jeff Karp Laboratory	N/A
LLC1 cell line	ATCC	ATCC® CRL-1642
Experimental Models: Organisms/Strains		
C57BL/6J	The Jackson Laboratory	000664
B6N.129S2-*Casp1*^{tm1Flv}/J (Casp1/11 $^{-/-}$)	The Jackson Laboratory	016621
B6.129S6-*Nlrp3*^{tm1Bhk}/J (NLRP3 $^{-/-}$)	The Jackson Laboratory	021302
B6 Ly5.1	The Jackson Laboratory	002014
B6(Cg)-*Zbtb46*$^{tm1(HBEGF)Mnz}$/J (Zbtb46^{DTR})	The Jackson Laboratory	019506
B6.Cg-*Gt(ROSA)26Sor*$^{tm1.1(CAG-Pycard/mCitrine*,-CD2*)Dtg}$/J (ASC-citrine)	The Jackson Laboratory	030744
B6.129S(C)-Batf3tm1Kmm/J	The Jackson Laboratory	013755
B6.129P2(C)-*Ccr7*^{tm1Rfor}/J	The Jackson Laboratory	006621
B6.SJL-*Ptprc*^{a}*Pepc*^{b}/BoyCrl (Ly5.1)	Charles River Laboratories	494

(*Continued on next page*)

Continued

REAGENT or RESOURCE	SOURCE	IDENTIFIER
C57BL/6J	Charles River Laboratories	027
BALB/c	The Jackson Laboratory	000651
Software and Algorithms		
GraphPad Prism 7.0	GraphPad Software	N/A
FlowJo (v10.3.0)	FlowJo	N/A
Microsoft Excel	Microsoft	N/A
Zen 2 Blue edition	Carl Zeiss Microscopy	N/A
Fiji / ImageJ version 2.0.0	https://imagej.net/Fiji	N/A
Other		
gentleMACS Dissociator	Miltenyi Biotec	130-093-235
Large Cell Columns	Miltenyi Biotec	130-042-401
MACSmix Tube Rotator	Miltenyi Biotec	30-090-753
Cytation Cell Imaging reader	BioTek instrument	N/A
5 mm Glass Diameter | Poly-D-Lysine Coated plates	Mattek	P96GC-1.5-5-F

RESOURCE AVAILABILITY

Lead Contact

Further information and requests for resources and reagents should be directed to and will be fulfilled by the Lead Contact, Jonathan C. Kagan (jonathan.kagan@childrens.harvard.edu).

Materials Availability

This study did not generate new unique reagents.

Data and Code Availability

The expression profiling by high throughput RNA sequencing generated during this study is available at GEO repository. The records have been assigned GEO accession numbers GSE156159.

EXPERIMENTAL MODEL AND SUBJECT DETAILS

Mouse strains, and Tumor cell lines

Female six- to eight-week old C57BL/6J, *casp1/-11*$^{-/-}$ mice, *Nlrp3*$^{-/-}$, *Casp11*$^{-/-}$, *Batf3*$^{-/-}$, *Ccr7*$^{-/-}$, B6 Ly5.1 (expressing the CD45.1 allele), *Zbtb46*^{DTR} mice bearing the human diphtheria toxin receptor under zinc finger and BTB domain containing 46, R26-CAG-ASC-citrine and BALB/c mice were purchased from Jackson Labs. Purchased mice were allowed to acclimate to the Boston Children's Hospital (BCH) housing facility for at least one week. For chimera mice experiments, four week old CD45.1 and C57BL/6J were used. In some experiments CD45.1, and C57BL/6 were purchased from Charles river and were housed in Mass General Hospital (MGH) animal facility. In all experiments, mice were randomly assigned to experimental groups. All experimental procedures were approved by the institutional animal care and use committee at BCH (IACUC 18-09-3796R) and MGH (IACUC 2005N000209 and 2014N000227). For syngeneic tumor models in C57BL/6J, two melanoma cell lines were used; the parental cell line: B16.F10 and an OVA expressing cell line B16.F10OVA from Dr. Arlene Sharpe (Harvard Medical School). For Lewis lung carcinoma model, LLC1 cells (obtained from ATCC) were used. For a syngeneic colorectal model, MC38 cell line expressing OVA derived from C57BL/6J murine colon adenocarcinoma cells were used and obtained from Dr. Arlene Sharpe (Harvard Medical School). For a syngeneic colon cancer model in BALB/c mice, CT26 cell line was used, and obtained from Dr. Jeff Karp (Harvard Medical School). These cells were cultured in DMEM containing 10% FBS, Penicillin and Streptomycin (Pen+Strep), and supplements of L-glutamine and sodium pyruvate. This media is referred to below as complete DMEM. Cell lines expressing the OVA protein were cultured in complete DMEM supplemented with puromycin (2 μg/ml).

Differentiation of GM-CSF- and FLT3L-BMDCs

B16 cell lines producing GM-CSF or FLT3L were cultured for approximatively 6 days in complete IMDM containing 10% FBS, Penicillin and Streptomycin (Pen+Strep) and supplements of L-glutamine and sodium pyruvate. This media is referred to below as complete IMDM. Supernatants were cleared of cellular debris by spinning at 400 x g for 5 min. Pooled supernatants from several culture

flasks were combined and passed through a 0.22 mm filter. GM-CSF and FLTL3L conditioned supernatants were aliquoted and frozen at −20°C. Leg bones were removed from mice, cut with scissors and flushed with sterile PBS pH 7.4 via syringe. Bone marrow suspension was passed through a cell strainer, resuspended in media consisting of complete IMDM with 10% of either GM-CSF or FLT3L conditioned media, then plated at $1x10^6$ bone marrow cells per untreated 10 cm dish. Plates were fed with 5mL of additional conditioned media on day 3 of differentiation. The efficiency of differentiation was monitored by flow cytometry using BD Fortessa and was routinely above 80%. Differentiated cells were used for subsequent assays on day 7 for GM-CSF-DCs and day 8 for FLT3L-DCs. BMDCs were washed with PBS and re-plated in complete IMDM at a concentration of $1x10^6$ cells/ml in a final volume of 100 μl.

METHOD DETAILS

Generation of full bone marrow chimeric mice for DC injections

To generate bone marrow chimeric mice using *Zbtb46*^{DTR} and WT mice, four week old CD45.1$^+$ female mice were irradiated with 1000 rads prior to their injection with bone marrow. Bone marrow was harvested from 8-11-week-old *Zbtb46*^{DTR} or WT mice by mechanical disruption using a mortar and pestle followed by incubation with RBC lysis buffer. Lysis was stopped by adding excess PBS, centrifugation and resuspension of the cell pellet in PBS. Within 6 hours of irradiation, recipient CD45.1 mice received a total of 0.7-1 × 10^7 bone marrow cells from WT or *Zbtb46*^{DTR} via retro-orbital injection in 100 μl. 6 weeks post reconstitution, recipient mice received 20ng/g per body weight of diphtheria toxin (DTx) intraperitoneally 3 times weekly for 2 weeks. DC depletion in the spleen and dLN was assessed 1-week post DT injection. These chimeric mice were used for DC injections in Figure S7 and were housed at MGH animal facility.

Generation of full or mixed bone marrow chimeric mice for immunizations

Four week old CD45.1$^+$ female mice were exposed to whole body irradiation (2 doses of 500 rads per mouse, 2 hours apart). After at least 4 hours from the last irradiation, mice were reconstituted with 5 × 10^6 bone marrow (BM) cells isolated from sex-matched mice and injected intravenously. Mice were kept in autoclaved cages and were treated with sulfatrim in the drinking water for 2 weeks after reconstitution. Then, mice were placed in standard cages and allowed to reconstitute for 6 more weeks. To evaluate the percentage of chimerism, peripheral blood samples were collected at the end of reconstitution and stained for CD45.1 and CD45.2. For these experiments, all mice were housed at the BCH animal facility.

To deplete conventional dendritic cells (cDCs), we generated full BM chimeras by reconstituting irradiated mice with BM cells isolated from *Zbtb46*^{DTR} mice. Reconstituted mice were injected intraperitoneally with saline (control mice) or diphtheria toxin (DTx, 400 ng per mouse) 3 times per week starting from 3 days post-tumor injection for a total of 6 DTx doses.

To specifically deplete selected genes in cDCs, we generated mixed BM chimeras by reconstituting irradiated mice with 4 × 10^6 BM cells isolated from *Zbtb46*^{DTR} mice mixed with 1 × 10^6 BM cells isolated from wild-type, *Nlrp3*$^{-/-}$, *Casp1/1*$^{-/-}$ or *Ccr7* $^{-/-}$ mice. Reconstituted mice were then injected intraperitoneally with DTx (400 ng per mouse as first dose, then 200 ng per mouse) 3 times per week starting from 12 days prior to tumor injection for a total of 9 (immunization experiments) or 12 (tumor challenge experiments) DTx doses.

Ligand and Chemical Reconstitution

E. coli LPS (Serotype O55:B5-TLR grade) was purchased from Enzo and used at 1 μg/ml in cell culture or 10 μg/mouse for *in vivo* use. In some experiments where indicated, LPS was used at 100ng/ml or 10ng/ml. Monophosphoryl Lipid A from *S. minnesota* R595 (MPLA) was purchased from Invivogen and used at 1 μg/ml in cell culture or 20 μg/mouse for *in vivo* use. CpG ODN 1826 used at 1 μg/ml in cell culture, was purchased from Invivogen. oxPAPC was purchased from Invivogen, resuspended in pre-warmed serum-free media and was used as 100 μg/ml for cell stimulation, or 65 μg/mouse for *in vivo* use. PGPC was purchased from Cayman Chemical. Reconstitution of PGPC was performed as previously described [26]. Briefly, ethanol solvent was evaporated using a gentle nitrogen gas stream. Pre- warmed serum-free media was then immediately added to the dried lipids to a final concentration of 1 mg/ml. Reconstituted lipids were incubated at 37°C for 5-10 mins then sonicated for 20 s before adding to cells. PGPC were used at 100 μg/ml for cell stimulation or 65 μg/mouse for *in vivo* use. In some experiments, oxPAPC or PGPC were used at concentrations ranging from 25 to 100 μg/ml. EndoFit chicken egg ovalbumin protein with endotoxin levels < 1 EU/mg and OVA 257- 264 peptide were purchased from Invivogen for *in vivo* use at a concentration of 200 μg/mouse or *in vitro* use at a concentration ranging from 1000 to 10 μg/ml. Incomplete Freund's Adjuvant (F5506) was purchased from Sigma and used for *in vivo* immunizations at a working concentration of 1:4 (IFA:antigen emulsion). Alhydrogel referred to as alum was purchased from Invivogen and used for *in vivo* immunization at a working concentration of 2mg/mouse. Where indicated, Addavax which is a Squalene-oil-in-water adjuvant was used instead of IFA at a working concentration of 1:2 (Addavax:antigen).

DC stimulation and T cell culture

To induce active DCs, DCs were stimulated in complete IMDM with LPS (1 μg/ml) for 15 or 18 or 24 hours as indicated. To induce hyperactive or pyroptotic DCs, cells were primed for 3 hours with LPS at a concentration of 1 μg/ml, unless otherwise indicated, then stimulated with oxPAPC or PGPC (100 μg/ml, unless otherwise indicated) or alum (100 μg/ml) for 12 or 15h or 21h as indicated. Naive DCs were cultured in the presence of complete media alone for the indicated time. T cells were cultured in RPMI-1640

supplemented with 10% FBS, 100 U/ml penicillin, 100 μg/ml streptomycin (Sigma-Aldrich), and 50 μM β-mercaptoethanol (Sigma-Aldrich). All cells were cultured at 37°C in a humidified atmosphere containing 5% CO2.

LDH Assay and ELISA

Fresh supernatants were clarified by centrifugation then assayed for LDH release using the LDH cytotoxicity colorimetric assay kit (ThermoFisher) following the manufacturer's protocol. Measurements for absorbance readings were performed on a Tecan plate reader at wavelengths of 490 nm and 680 nm. To measure secreted cytokines, supernatants were collected, clarified by centrifugation and stored at −20°C. ELISA for IL-1β, TNFα, IFNγ, IL-2, were performed using eBioscience Ready-SET- Go! (now ThermoFisher) ELISA kits according to the manufacturer's protocol.

Antigen uptake and peptide presentation assay

To examine antigen uptake and the endocytic ability of BMDCs, Alexa Fluor 488 labeled-chicken OVA (AF488-OVA) was used (ThermoFisher). Briefly, naive, active, pyroptotic or hyperactive FLT3L-derived BMDCs previously cultured with media alone, or treated for 24 hours with LPS alone or in combination with PGPC or alum, were incubated with AF488-OVA (0.5 mg/ml) for 45 minutes at 37°C, or at 4°C (as a control for surface binding of the antigen). BMDCs were then washed and stained with Live/Dead Fixable Violet dye (ThermoFisher) to distinguish living cells from dead cells. Cells were then fixed with BD fixation solution and resuspended in MACS buffer. FITC fluorescence of live cells was measured. Fluorescence values of BMDCs incubated at 37°C were reported as Mean fluorescence Intensity (MFI) of OVA-AF488 associated cells as normalized to MFI of OVA-AF488 associated cells incubated at 4°C.

To measure the efficiency of OVA peptide presentation on MHC-I, FLT3L-derived BMDCs were treated as described above and incubated with Endofit-OVA protein (0.5mg/ml) for 1 hour at 37°C. Cells were then washed with MACS buffer and stained at 4°C for 20 to 30 minutes with APC-conjugated anti-mouse H-2K^{b} antibody (BioLegend), and a PE-conjugated antibody that binds to H-2K^{b} bound to the OVA peptide SIINFEKL (BioLegend). Non-OVA-treated DCs served as a negative control and isotype controls were used as a staining control. The percentage of total surface H-2K^{b}, and the percentage of cells associated with the OVA peptide on MHC-I was calculated. Data were acquired on a Fortessa flow cytometer (Becton-Dickenson) and analyzed with FlowJo software (Tree Star).

DC injections for DC migration assay

BMDCs generated using FLT3L were prepared from C57BL/6J mice (on a CD45.2 background), harvested on day 8 and suspended at a concentration of 1x10^{6} cells/ml in complete IMDM. DCs were either left untreated or treated with LPS alone for 15 hours, or BMDCs were primed with LPS for 3h then treated with PGPC or oxPAPC or alum for 12h. Alternatively, BMDCs from *Nlrp3*$^{-/-}$ or *Ccr7*$^{-/-}$ or ASC-citrine mice were primed with LPS for 3h then treated with PGPC for 12h. DCs were cultured in polypropylene tubes with gentle rotation using MACSmix Tube Rotator (Miltenyi Biotec) in the incubator. Cells were washed, stained for 30 minutes with CFSE, and then 1x10^{6} live DCs were injected s.c. on the right flank into ly5.1/CD45.1 mice in a total volume of 100 μl. 15 hours post DC injection, single cell suspension from the skin draining lymph nodes were stained with live-dead violet dye in PBS, then washed and stained in MACS buffer with anti-CD11c, anti-CD45.1 and anti-CD45.2 antibodies (BioLegend). Uninjected mice (no DCx) served as a control. Hyperactive DCs that migrated to the dLN were sorted as CFSE^{+} CD45.2^{+} CD11c^{+} live cells, and resident DCs were sorted as CFSE^{neg} CD45.1^{+} CD11c^{+} live cells. Sorted cells were cultured in media alone for 24 hours onto 96-well round bottom plates. Supernatants were used for LDH and IL-1β cytokine release as described above. For ASC microscopy experiments using migrated DCs in the dLN, WT or *Nlrp3*$^{-/-}$ DCs were injected as mentioned above without CFSE staining.

Microscopy Imaging

For DC immunostaining, DCs generated using FLT3L were cultured on coverslips and either left untreated (none) or treated with LPS alone for 18 hours, or BMDCs were primed with LPS for 3h then treated with PGPC or Alum for 15h. Cells were washed then fixed with 4% PFA for 15 minutes at room temperature, and blocked using 1% goat serum for 1 hour. For immunofluorescence staining of hyperactive DCs that migrated to the dLN, cells were sorted from the dLN as CD11c^{+} CD45.2+ CD45.1^{-} CFSE^{+} live cells and plated onto glass 96 well plates. DCs were stained with iFluor 488 phalloidin (ThermoFisher) and DAPI. For anti-ASC speck staining, hyperactive DCs were sorted from the dLN as CD11c^{+} CD45.2+ CD45.1^{neg} and resident DCs as CD11c^{+} CD45.2^{neg} CD45.1^{+} then plated on glass 96 wells flat plate. Cells were left to rest in media for 3-4hours, then fixed using 4% PFA. DCs were stained with Alexa Fluor 647 conjugated Phalloidin (ThermoFisher), rabbit anti-ASC (Adipogen) followed by Alexa Fluor 488-conjugated chicken anti-rabbit IgG (ThermoFisher). ASC-citrine hyperactive DCs or resident DCs were sorted from the dLN then fixed with 4% PFA for 15 minutes at room temperature, blocked using 1% goat serum for 1 hour, then stained with Alexa Fluor 647 conjugated Phalloidin and DAPI. Images were acquired using 20x or 63x oil immersion lenses on Zeiss microscope.

Cell tracking and time-series analysis

8 days old FLT3L-DCs were cultured as described above for 15 hours in media alone or in the presence of LPS, or upon priming with LPS for 3 hours followed by PGPC treatment for 12 hours. Cells were washed twice with PBS then plated onto glass plates for 3 hours to rest prior to Image acquisition on BioTek instrument. Images were acquired every 2 minutes for 5 consecutive hours. Image

processing and cell tracking were performed for 4 independent ROI using the image-processing software Fiji (Schindelin et al., 2012). The recorded time-series were imported using the Bio-Formats plugin (Linkert et al., 2010) and cell tracks were manually tracked using the Manual Tracking plugin (Fabrice Cordelieres). Floating and dead cells were not tracked. Positional data was then imported into R and individual cell statistics were calculated (https://cran.r-project.org/web/packages/data.table/index.html; https://cran.r-project.org/web/packages/dplyr/index.html). Cell tracks were visualized using the ggplot2 package.

Flow cytometry and cell sorting

After FcR blockade, treated FLT3L-BMDCs were washed and stained in PBS with Live Dead Fixable dye (ThermoFisher) for 20 minutes at 4°C. Cells were then washed again and stained for 20 minutes at 4°C in MACS buffer (PBS with 1% FCS and 2 mM EDTA) containing the following fluorescently conjugated antibodies purchased from BioLegend: anti-CD11c, anti-I-A/I-E, anti-H-2Kb, and anti-CCR7. For cDC1 and cDC2 sorting, FLT3-derived DCs were stained for 20 minutes at 4°C with monoclonal anti-SIRP alpha (eBioscience), anti-mouse CD24 (BioLegend), monoclonal anti-CD11c (ThermoFisher), anti-mouse MHC Class II (VWR), anti-mouse CD45R (BD), anti-CD64 (BD) and monoclonal anti-F4/80 antibody (ThermoFisher). To assess DC depletion in the dLN following diphteria toxin treatment, single cell suspension forms the dLN were stained with following antibodies (BioLegend): anti-CD45.1, anti-CD45.2, anti-MHC-II, anti-CD11c, and anti-CD64 (BD), and monoclonal anti-F4/80 antibody (ThermoFisher).

Single cell suspension from the tumor or draining inguinal lymph nodes, or spleen, or skin inguinal adipose tissue or skin biopsies were stained for 20 minutes in PBS at 4°C with Live Dead Fixable Violet or green dye (ThermoFisher) to determine the viability of cells prior to antibodies staining. Cells were washed then resuspended in MACS buffer (PBS with 1% FCS and 2 mM EDTA) and stained for 20 minutes at 4°C with the following fluorescently conjugated antibodies (BioLegend): anti-CD8α, anti-CD4, anti-CD44, anti-CD62L, anti-CD3, anti- CD103, anti-CD69, anti-CD45. For antigen-specific T cell detection, T cells were stained with OVA-peptide tetramers at room temperature for 1h. PE-conjugated H2K(b) SIINFEKL and APC conjugated I-A(b) AAHAEINEA (OVA 329-337) were used. I-A(b) and H2K(b) associated with CLIP peptides were used as isotype controls. Tetramers were purchased for NIH tetramer core facility. For tetramer staining, FITC anti-CD8.1 was purchased from accurate chemical.

For intracellular cytokine staining, T cells were stimulated with 50ng/ml phorbol 12-myristate 13-acetate (PMA) and 500ng/ml ionomycin (BioLegend) in the presence of GolgiStop and brefeldin A for 4-5 h. Cells were then washed twice with PBS, and stained with LIVE/DEAD Fixable violet Stain Kit (ThermoFisher) in PBS for 20 min at 4°C. T cells were then washed with MACS buffer, and stained for appropriate surface markers as described above. After two washes, cells were fixed and permeabilizated using BD Cytofix/Cytoperm kit for 20 min at 4°C, then washed with 1X perm wash buffer (BD) per manufacturer's protocol. Intracellular cytokine staining was performed in 1X perm buffer for 20- 30 min at 4°C using anti-IFN-γ (BioLegend). Data were acquired on a BD FACS ARIA or BD Fortessa. Data were analyzed using FlowJo software.

To determine the absolute number of cells, countBright counting beads (ThermoFisher) were used, following the manufacturer's protocol. Appropriate isotype controls were used as a staining control. Data were acquired on a BD FACS ARIA or BD Fortessa (Becton-Dickenson). Data were analyzed using FlowJo software (Tree Star).

Adoptive DC transfers

For DC transfers, BMDCs generated using FLT3L were harvested on day 8, and suspended at a concentration of $1x10^6$ cells/ml in complete IMDM. DCs were treated as described above for 18 hours prior to their injection into recipient mice. DCs were cultured in polypropylene tubes with gentle rotation using MACSmix Tube Rotator (Miltenyi Biotec) in the incubator. 18 hours post-culture, DCs were washed twice with PBS, counted using trypan blue (GIBCO), then loaded (or not) with antigens such as OVA (serial dilution starting 500 ug/ml) or whole tumor lysates for 1 hour. DCs were washed twice again with PBS and $1x10^6$ cells in 100ul were injected subcutaneously on the right flank of recipient mice. For DC-based immunotherapy experiments, recipient mice received the first DC injection when tumors reached 3-4 mm of size, followed by 2 DC injections every 7 or 10 days.

DC and antigen-specific $CD8^+$ T cell coculture

8 weeks old female mice were s.c. immunized with OVA antigen emulsified in IFA on the right back. 7 days later, mice received a boost injection with OVA antigen emulsified in IFA on the left back. 14 days after the first immunization, splenic $CD8^+$ T cells were sorted from immunized mice by magnetic cell enrichment using anti-CD8 beads. Total $CD8^+$ T cells were sorted with a purity above 98%. The percentage of $SIINFEKL^+$ $CD8^+$ T cells was assessed by flow cytometry using tetramer staining and was estimated around 1%–2% among total $CD8^+$ T cells. Total $CD8^+$ T cells were seeded in 96-well plates at a concentration of 10^5 cells per well in the presence of $1x10^4$ DCs (10:1 ratio). 7 days post culture, supernatants were collected and clarified by centrifugation for short-term storage at −20°C and cytokine measurement by ELISA. Cells were then processed as described above for an intracellular staining.

In vivo immunization and T cell re-stimulation

8 weeks old female mice were immunized subcutaneously (s.c.) on the right flank with either 200 μg/mouse endotoxin-free OVA alone or with 10 μg/mouse LPS emulsified in incomplete Freund's adjuvant. Alternatively, mice were immunized with 200 μg/mouse endotoxin-free OVA, plus 65 μg/mouse oxPAPC or PGPC, plus 10 μg/mouse LPS emulsified in incomplete Freund's adjuvant. In some experiments, mice were injected s.c. with OVA plus LPS emulsified in alum. 7 or 40 days after immunization, $CD8^+$ T cells were isolated from the skin draining lymph nodes of immunized mice by magnetic cell sorting with anti-CD8 beads. Enriched cells were then

sorted as live $CD45^+CD3^+CD8^+$ cells. Purity post-sorting was > 98%. Sorted cells were then seeded in 96-well plates in the presence of OVA-preloaded BMDC (at a ratio of 1 DC: 10 T cells). Secretion of IFNγ was measured by ELISA 5 days later. In some experiments, the percentage of antigen-specific T cells expressing IFNγ was measured by intracellular staining 5 days post-co-culture.

CD107a degranulation assay

$CD8^+$ T cells from the skin draining lymph nodes of immunized mice were isolated by magnetic cell enrichment with anti-CD8 beads, then sorted as $CD45^+CD3^+CD8^+$ cells live cells. Freshly sorted $CD8^+$ T cells were resuspended in complete RPMI at a concentration of $1x10^6$ cells/ml. anti-CD107a (LAMP-1) antibody (BioLegend) was added to this media at a concentration of 1 μg/ml, in the presence of GolgiStop. T cells were then immediately seeded in 96 wells plate at a concentration of 100,000 cells in the presence of 10,000 B16OVA as target cells. Alternatively, $CD8^+$ T cells were seeded alone and stimulated for 5 hours with 50 ng/ml phorbol 12-myristate 13-acetate (PMA) and 500 ng/ml ionomycin (Sigma-Aldrich). 5 hours post-culture, cells were washed with MACS buffe r, stained with LIVE/DEAD Fixable Violet Dead Cell Stain Kit (Thermofisher), and anti-CD8 (BioLegend). Cells were then Fixed with BD fixation solution for 20 min at 4°C and resuspended in MACS buffer. The percentage of $CD107a^+$ $CD8^+$ T cells was determined by flow cytometry on the Fortessa flow cytometer (BD).

In vitro cytotoxicity assay

$CD8^+$ T cells from the spleen, or the skin inguinal adipose tissue of survivor mice were isolated using anti-CD8 MACS beads. Enriched T cells were then sorted as live $CD45^+CD3^+CD8^+$ cells. Purity post-sorting was > 97%. B16OVA, B16F-10 or CT26 tumor cells were seeded onto 96-well plates ($1x10^4$ cells/well) in complete DMEM at least 5 hours prior their co-culture with T cells. 10^5 $CD8^+$T cells were seeded onto tumor cells for 12h, then cytotoxicity was assessed by LDH release assay using the LDH cytotoxicity colorimetric assay kit (ThermoFisher) following the manufacturer's protocol.

Whole tumor lysates preparation

To prepare whole tumor cell lysates (WTL) for prophylactic immunization, tumor cell lines were cultured for 4- 5 days in complete DMEM. When cells became confluent, supernatants were collected, and the cells were washed and dissociated using trypsin-EDTA (GIBCO). Tumor cell lines were then resuspended at $5x10^6$ cells/ml in their collected culture supernatant, then lysed by 3 cycles of freeze-thawing. For immunotherapy experiments, syngeneic WTL were prepared from tumors explants of unimmunized tumor-bearing mice. Briefly, tumors from unimmunized mice bearing a tumor 10-12 mm of size were mechanically disaggregated using gentleMACS dissociator (Miltenyi Biotec) and digested using the tumor Dissociation Kit (Miltenyi Biotec) following the manufacturer's protocol. Tumors were incubated for 45 minutes at 37 degrees in a tube rotator for complete digestion. After digestion, tumor cell suspensions were washed with PBS and passed through 100-μm then 70-μm then 30-μm filters. Single cell suspension was depleted of $CD45^+$ cells using anti-CD45 TILs microbeads (Miltenyi Biotec). Tumor cells were then counted and resuspended at $5x10^6$ cells/ml then lysed by 3-4 cycles of freeze-thawing. All prepared Lysates were centrifuged at 12,000 rpm for 15 minutes, and supernatants were passed through 70-μm and 30-μm filters then stored in aliquots at −20°C until use. WTL were used for immunotherapy or for BMDC antigen loading at a concentration equivalent to $2.5x10^5$ tumor cells per mice, or at ratio equivalent to 1:10 (DC:tumor cells) respectively.

Prophylactic immunization and tumor challenges

For immunizations prior to tumor inoculation, mice were injected subcutaneously (s.c.) into the right flank with PBS (unimmunized), WTL alone at a concentration equivalent to $2.5x10^5$ tumor cells per mice or with WTL plus 10 μg/mice of LPS, or WTL plus LPS plus 65 μg/mice of oxPAPC or PGPC, all emulsified in incomplete Freud's adjuvant (IFA). In some experiments, LPS is replaced by MPLA. 15 days post immunization, mice were challenged s.c. on the left flank with $3x10^5$ of viable B16OVA cells, or $5x10^5$ of viable MC38-OVA cells, as indicated. Tumor-free mice were re-challenged s.c. into the upper back with a lethal dose of $6x10^5$ viable B16OVA or $1x10^6$ of viable MC38-OVA cells, as indicated. When indicated, mice were given 100 μg of LEAF anti-mouse/rat IL-1β antibody (BioLegend) by intravenous (i.v.) injection for five consecutive days; starting two days before receiving the immunization, then on day 1, day 2, and day 3 post-immunization to ensure chronic depletion of circulating IL-1β. The size of the tumors was assessed in a blinded, coded fashion every two days and recorded as tumor area (length × width) using a caliper. Mice were sacrificed when tumors reached 2 cm^3 or upon ulceration.

Immunotherapeutic immunization and tumor challenges

For immunizations in the context of an immunotherapeutic approach, C57BL/6J were injected on the left flank with $3x10^5$ of viable B16OVA cells, or $3x10^5$ of B16-F10 cells, or $5x10^5$ of viable MC38-OVA cells, or $3x10^5$ of LLC1 cells. Alternatively, BALB/c mice were injected on the left flank with 3x105 of viable CT26 cells. When tumors reached 3-4mm of size, mice were either left untreated (unimmunized) or injected intraperitoneally (i.p.) with 100 μg of anti-PD-1 every two days for 5 consecutive injections. Alternatively, mice were immunized with WTL at a concentration equivalent to $2.5x10^5$ tumor cells per mice plus 10 μg/mice of LPS and 65 μg/mice of PGPC emulsified in incomplete Freud's adjuvant (IFA). Immunizations were followed by two boost injections every 7-10 days. Immunized mice were divided blindly into several groups. Some mice were injected i.p. with 100 μg of Ultra-LEAF anti-CD4, or CD8a starting the day of immunization or the day of boost injection, followed by 3 consecutive injections every 2 days. Other mice were given

100 μg of LEAF anti-mouse/rat IL-1β antibody or IL-1 receptor antagonist (IL1RA) by i.v. injection every day for five consecutive days; starting two days before receiving the immunization, then on day 1, day 2, and day 3 post-immunization to ensure chronic depletion of circulating IL-1β. The injection of anti-IL-1β antibody or IL1RA were repeated for every boost injection. Control mice received isotype-matched rat IgG. All antibodies were purchased from BioLegend, and IL-1RA was purchased for Cayman Chemical. The size of the tumors was assessed in a blinded, coded fashion every two days and recorded as tumor area (length × width) using a caliper. Mice were sacrificed when tumors reached 2 cm^3 or upon ulceration.

Tumor infiltrating T cells in the tumor microenvironment

To assess the frequency of tumor-infiltrating lymphocytes (TILs) in the tumor microenvironment (TME), mice were dissected and peri-tumoral tissue was discarded. Tumors were harvested then dissociated using the tumor Dissociation Kit and the gentleMACS dissociator (Miltenyii Biotec), following the manufacturer's protocol. After digestion, tumors were washed with PBS and passed through 70-μm and 30-μm filters. $CD45^+$ cells were positively selected using anti-CD45 TILs microbeads (Miltenyi Biotec). In prophylactic immunization experiments, the frequency of $CD4^+$ T cells and $CD8^+$ T cells was calculated among $CD3^+$ $CD45^+$ single live cells. In LLC1 tumor model experiments, $CD8^+$ T cell infiltration and T resident memory $CD8^+$ T cells in the TME defined as $CD103^+CD69^+$ $CD8^+$ T cells were calculated among $CD45^+$ $CD8^+CD11b^{neg}$ $CD19^{neg}$ single cells. Tumor infiltrating $CD45^+$ cells were cultured for 24 hours with dynabeads mouse T-Activator CD3/CD28 (ThermoFisher) for T cell activation and IFN-γ measurement.

In vivo immunization and B16-F10 pulmonary colonization

To induce experimental lung colonization, $3x10^5$ B16-F10 tumor cells were injected intravenously (i.v.) via tail vein in a volume of 100 ul. 2 days before tumor inoculation, mice were left untreated (unimmunized) or were immunized subcutaneously (s.c.) on the right flank with WTL alone or with LPS, or with WTL plus LPS and PGPC, all emulsified in Addavax. Mice received a boost injection 5 days post tumor inoculation. Mice were then sacrificed on day 18 after tumor cell injection, and lung tissues were isolated and fixed. Lung metastatic nodules present on the surface of the lungs per mouse were enumerated.

Skin biopsies and skin adipose tissue dissociation

Skin punch biopsies were performed at the site of immunization and tumor injection site of survivor mice. Skin was incubated in Dispase solution (Roche, 2.5 mg/ml) for 90 minutes and the epidermis separated from the dermis. The dermis was chopped finely and incubated in collagenase type III (Sigma, 3 mg/ml) and the epidermis placed in trypsin/EDTA (Sigma) and incubated at 37°C for 30 min. For adipose tissue dissociation, tissues were chopped using scissors and dissociated using gentleMACS dissociator (Miltenyi Biotec) in the presence of collagenase A (Sigma, 3 mg/ml), then incubated in a tube rotator for 30 minutes 37°C. Cells were passed through 70-μm and 30-μm filters, and centrifuged for 10 minutes at 1300rpm. The lipid layer was aspirated, and supernatants discarded. Cells were then treated with ACK lysis solution for 5 minutes at 4°C. Single cell suspension from the skin tissue or skin adipose tissue were suspended in MACS buffer for staining.

Adoptive T cell transfer

For T cell transfer, T circulating $CD8^+$ T cells from the spleen, or T resident memory cells from the skin inguinal adipose tissue of survivor mice were isolated using anti-CD8 MACS beads (Miltenyi Biotec). Enriched cells were then sorted as live $CD45^+CD3^+CD8^+$ cells using FACS ARIA. Purity post-sorting was > 97%. Sorted T cells were then stimulated for 24 h in 24-well plates (~2×10^6 cells/well) coated with anti-CD3 (4 μg/ml) and anti-CD28 (4 μg/ml) in the presence of IL-2 (Peprotech, 50ng/ml). $5.x10^5$ of activated splenic or skin inguinal adipose $CD8^+$T cells were transferred by i.v. or intra dermal (i.d.) injection respectively on the right flank into naïve recipient mice 7 days prior tumor challenge. Some mice received both T cell subsets 7 days prior tumor challenge.

RNA sequencing

RNA was extracted using RNeasy Plus Micro kit (QIAGEN) following the manufacturer's protocol. cDNA was produced from isolated RNA with the Smart-Seq2 reverse-transcription protocol as described by Picelli et al. (2014) with the following modifications: 1) Concentrations of input RNA was normalized to ~2,000 cells-worth of input RNA per reaction. 2) The Superscript II reverse-transcription enzyme was replaced with Superscript III (ThermoFisher, #18080-085) which was applied according to manufacturer's instructions. Paired-end sequencing libraries were generated from cDNA with the Nextera XT DNA sample Prep Kit (Illumina, #FC-131) according to the manufacturer's instructions. Libraries were pooled at an equimolar ratio and sequenced on a NextSeq500/550 sequencer (Illumina) using a 75 cycle v2.5 sequencing kit with a paired end read structure. Following sequencing, runs were demultiplexed using bcl2fastq v2.2 then aligned with HISAT2 (Kim et al., 2015) against GRCm38 and quantified with RSEM (Li and Dewey, 2011) generating a gene by sample count matrix further analyzed with Seuratv3 (Stuart et al., 2019) and DESeq2 (Love et al., 2014). Treatment based pairwise differential expression was calculated with DESeq2′s negative binomial expression tests grouped by FLT3L-cDC1 and FLT3L-cDC2 populations. The significance threshold was set at 0.05 and multiple expression tests were accounted for with Bonferroni p value correction. Gene set module scores are calculated from the average expression levels of each module on a per sample basis and subtracted by the baseline expression of randomly selected gene sets of same size using Seurat's AddModuleScore function. One gene set (Curated Cell Migration Module) was curated based genes found to be significantly differentially expressed within

LPS plus PGPC versus LPS treatment in FLT3L cDC1 and FLT3L cDC2 populations. Other gene sets were selected from the Gene Ontology database (http://www.informatics.jax.org/vocab/gene_ontology/). All genes used within each module are provided within Table S1.

QUANTIFICATION AND STATISTICAL ANALYSIS

In *in vivo* studies, n refers to the number of animals per condition from at least 2 independent experiments. Statistical differences were calculated by using unpaired two-tailed Student's t test, or one-way ANOVA with Tukey post- test. Dependent samples were analyzed with paired t tests. Statistical significance for experiments with more than two groups was tested with two-way ANOVA with Tukey multiple comparison test correction. All experiments were analyzed using Prism 7 (GraphPad Software). Graphical data was shown as mean values with error bars indicating the SD or SEM. P values of < 0.05 (*), < 0.01 (**) or < 0.001 (***) ; ≤ 0.0001 (****) indicated significant differences between groups